ΠΑΝΕΠΙΣΤΗΜΙΟ ΚΡΗΤΗΣ
UNIVERSITY OF CRETE

Simulation of neuronal dynamics using Josephson junctions

Dimitris Chalkiadakis

Supervisor: Johanne Hizanidis (Ioanna Chitzanidi)

June 2021

Acknowledgement

I would like to express my deepest gratitude to my Supervisor Dr. Johanne Hizanidis for the continuous support of my B.Sc. study and research, for her patience and her insightful comments. Her guidance was invaluable throughout the entire research and thesis writing process.

I would also like to thank the other members of my Examination Committee Dr. Philipp Hoevel and Dr. Konstantinos Makris for dedicating their time in order to examine this B.Sc. thesis.

Contents

Chapter 1

Introduction

1.1 Neuromorphic Computing

Computers have long ago surpassed humans in computation capabilites in terms of speed and precision. Until recently, however, they were not able to solve problems, at which humans excel, for instance distinguishing between pictures depicting cats and dogs. The last 20 years this situation has changed due to the employment of brain inspired algorithms, such as deep neural networks. Nonetheless, computers need great amount of energy and, in some cases, time compared to their biological counterparts. For example, a state of the art natural language processing model consumes 1,000kWh when trained on a supercomputer, while the same amount of energy is enough for a human brain to function for 6 years [1].

The brain is fundamentally different from a computer. It consists of highly interconnected neurons which communicate with each other through adaptive synapses, by exchanging digital signals (spikes), while they perform analogue computation of the received signals at their cell somas. Furthermore, neurons work in parallel, without using a perfectly synchronous clock and they produce spikes only when the input signals force them to, resulting in low energy dissipation. Finally, in biological neural networks, the memory and the processing units, which correspond to synapses and neurons respectively, are not separated. Computers on the other hand, spend time and energy in order to move data from the memory to the processors and vice versa, the so called "von Neumann bottleneck". For this reason, standard computers and supercomputers waste an important part of their resources

when a neural network is involved. This affects both the operation of artificial neural networks during the phases of training and inference, and the study of biological neural networks through simulations.

Platform:	Human brain	BrainScaleS	SpiNNaker
# neurons:	100 B	4 M	460 M
# synapses:	10^{15}	1 B	460 B
power:	20 W	10 kW	50 kW
Energy/connection:	10 fJ	100 pJ	10 nJ
Speed versus biology:	1×	10 000×	1×
Interconnect:	3D direct signalling	Hierarchical	2D mesh-multicast

Figure 1.1: Comparison between the brain and two famous neuromorphic systems based on CMOS technology. Adapted from [2].

The science of neuromorphic computing aims to tackle these problems by employing brain inspired architecture and hardware. It has been supported, however, that the transition to more spiking friendly hardware demands the use of new devices in the fundamental level because it is impossible to achieve the interconnectedness and the energy efficiency of the brain with the technology of the superconductors. A typical neuron made from complementary metal–oxide–semiconductor (CMOS) transistors has many components and suffers from energy dissipation. Moreover, the circuitry is confined in two dimensions reducing the number of connections a neuron can have [1]. Figure 1.1 shows that two of the most complex neuromorphic systems based on CMOS technology existing today, use much more power while containing orders of magnitudes less neurons and synapses than a single brain [2]. A great variety of different physical systems and materials has been proposed which are able to simulate biological neurons at some level, due to their intrinsic properties [1]. Some of them are depicted in Fig. 1.2, along with their advantages and disadvantages.

Neuromorphic computing is divided in two approaches. The first one, tries to replace the standard hardware, such as graphical processing units (GPUs) or tensor processing units (TPUs) with more efficient ones, for the needs of the artificial intelligence (AI). On the other hand, the second approach, which is the one that this thesis follows, aims to bring closer the hardware to the biological brain, from the lower level, that is, the neuron,

Technology	CMOS synapses and neurons	Resistive switching synapses with CMOS neurons	Photonic synapses and neurons	Spintronic synapses and neurons	Superconductive synapses and neurons
Connections	Wires	Wires	Light	Microwaves	Wires or microwaves
Minimum lateral size of neuron	10 µm	10 µm	100 µm	10 nm	20 nm
Minimum lateral size of synapse	10 µm	10 nm	1 µm	10 nm	20 nm
Advantages	Commercially available	Nanoscale synapse, technology ready	Wavelength multiplexing, can be completely passive (low energy consumption[150,151])	Nanoscale synapses and neurons, almost commercial technology	Low energy consumption beside cryogenic requirements, all identical spikes
Disadvantages	Size of neurons and synapses, no in-memory computing	Size of neurons, complex wiring	Size of neurons and synapses, dissipation required for nonlinearity	Scalability yet to be demonstrated	Scalability yet to be demonstrated
Chip capabilities	Inference and learning	Inference	No chip	No chip	No chip

Figure 1.2: Comparison between different neuromorphic systems. Adapted from [1].

to the higher. In this way it integrates neuroscience-inspired concepts which are not taken into account by classical AI algorithms, intending to enhance our knowledge for the learning process of both machines and humans.

1.2 Superconducting neuromorphic devices

Devices consisting of superconducting materials are praised for their quick and competitive energy performances even with the required cryogenic conditions taken into account. The neuromorphic neurons in this field are based on two different materials: Josephson junctions and shunting nanowires [3, 4]. The former case has been studied more though the latter seems very promising. In principle, it has been demonstrated that neurons based on these materials are able to communicate with each other, even though their operation is based on different mechanisms, while the shunting nanowire neuron integrates easily with existing CMOS circuitry [5].

This thesis is concerned with neurons made of Josephson junctions (JJ neuron), and more specifically with those that mimic a spike with a single-flux-quantum-pulse (SFQ pulse). The research in this field, following the second approach to neuromorphic computing, has demonstrated that a JJ neuron exhibits fundamental neurocomputational properties such as refractory period, firing thresholds and classes 1 and 2 of excitability [6]. Furthermore, a neural network of 2 coupled JJ neurons has been manufactured in order to determine the role of the synaptic strength and delay in the synchronization. This neuromorphic experiment needs around 7000 less time that it

would if only digital approaches are used, suggesting that superconducting neurons can become a feasible tool in neuroscience [7].

1.3 Thesis goal

The realistic emulation of biological neurons using Josepshon junctions is an ambitious project due to the fact that both systems are complex and they are described by different laws. The language of dynamical systems can act as a bridge between these two diverse fields. The goal of this thesis is to elucidate the dynamics of the JJ neuron and compare them with the neuronal ones, continuing previous works [6]. This way, we will be able to identify which neurocomputational properties are exhibited by the JJ neuron and which are not. In addition, some cases will be demonstrated, where the JJ neuron exhibits behaviour beyond the realistic neuronal one. This is an important step before more research is conducted in the collective behaviour of JJ neurons.

The thesis is organized as follows:

Chapter 2 – Biological Background. In this chapter, we explain the generation of a spike in biological neurons. We also introduce the Hodgkin-Huxley model, the first neuronal dynamical model.

Chapter 3 – Dynamical Background. This chapter introduces the basic dynamical notation. Furthermore, we explain the analytical and computational tools which will be used. Finally, we present some fundamental neurocomputational properties and their dynamical equivalent.

Chapter 4 – Josephson Junction Neurons. The JJ neuron is introduced and the equations describing the systems are derived.

Chapter 5 – Mathematical analysis. In this chapter we present the results of our work. The equations are analyzed with analytical and computational tools. Moreover, we state which neurocomputational properties can be exhibited by a JJ neuron.

Chapter 6 – Conclusion and outlook. The results are summarized and possible future work is discussed.

Chapter 2

Biological Background

2.1 Biological neurons

Neurons are the elementary processing unit of the nervous system. A typical simplified neuron consists of 3 different parts with distinct computational properties. Signals from other neurons are received in branched processes called dendrites. Then, they are transmitted to the cell soma which acts as a processing unit, where a new signal (or spike) can be generated depending on the input. Lastly, the axon is responsible for transmitting the new signal to other neurons [8].

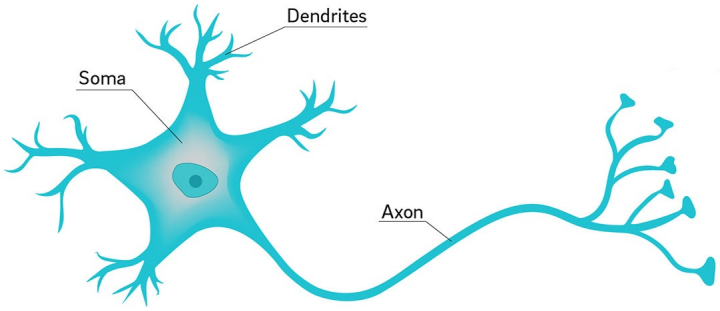

Figure 2.1: Simplified schematic of neuron.

Each neuron is highly interconnected with up to 10^4 other cells. Signals are transmitted through synapses which are found at the dendrites and at the end of the axon.

Due to the fact that the decision to fire or not and the generation of the spike happens at the soma, our analysis concerns only this part of the neuron,

although circuits simulating the axon and the synapses have been proposed too [6].

2.2 Action Potentials

Neuronal signals consist of spikes of the potential of the cellular membrane which are generated by inward and outward movement of ions through ionic channels [9]. These spikes are also called Action Potentials (AP). An AP is generated from the interplay of at least 2 ionic currents with Na^+ and K^+ being the major ones.

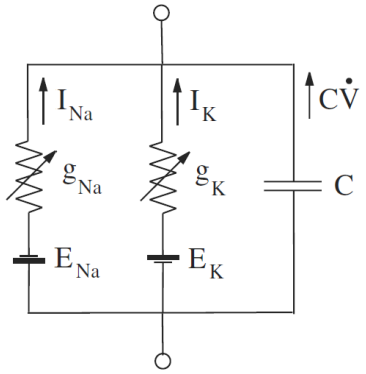

Figure 2.2: Equivalent circuit. C denotes the capacitance of the membrane, E_{ion} and g_{ion} denotes Nernst potential and the nonlinear resistance for each ion respectively. Taken from [9].

Each ion tries to balance electrical and chemical forces due to its charge and uneven concentration across the membrane. The equilibrium potential for a given ion is provided by the Nernst equation.

$$E_{ion} = \frac{RT}{Fz} \log \frac{C_{ion,out}}{C_{ion,in}}, \tag{2.1}$$

where R is the ideal gas constant, T is the absolute temperature, F is the Faraday constant, z is the electrical charge and C the concentration of an ion. When the membrane potential is equal to the Nernst potential of an ion, then no current of this ion can flow through the membrane. For a

different potential V, ionic current flows across the membrane according to the equation:

$$I_{ion} = g_{ion}(V - E_{ion}), \tag{2.2}$$

where g_{ion} denotes conductance. Na^+ and K^+ have opposite equilibrium potentials $E_{Na^+} \approx 60$ and $E_{K^+} \approx -90$ which is crucial for the generation of spikes. The physical meaning of conductance is how many ionic channels are in the open state. The electrical properties of membranes can be represented by an equivalent circuit, as shown in Fig. 2.2.

According to Kirchhoff's laws when an external current I passes through the equivalent circuit, the potential across the capacitance reads:

$$C\frac{dV}{dt} = I - g_{Na^+}(V - E_{Na^+}) - g_{K^+}(V - E_{K^+}). \tag{2.3}$$

APs are generated because g_{Na^+}, g_{K^+} are non linear functions of voltage. Biologically this results from ionic channels being controlled by gating particles which can be more than one and have different responses to the membrane potential, as shown in Fig. 2.3.

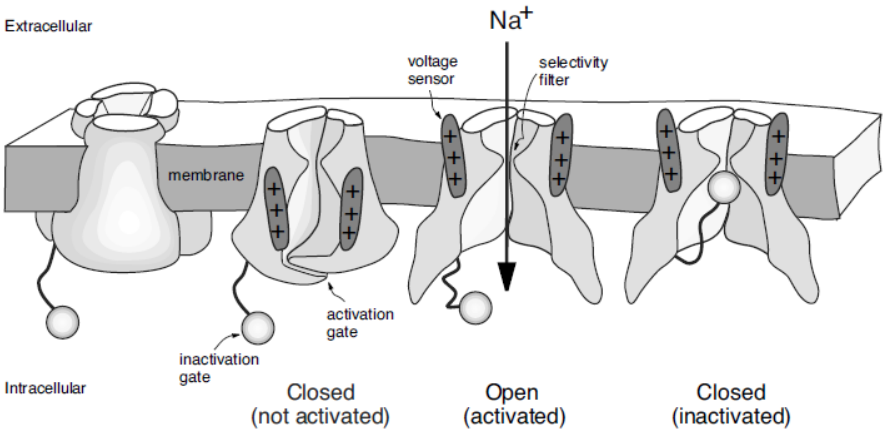

Figure 2.3: Different states of a Na^+ channel with one activation and one inactivation channel. Taken from [9].

Figure 2.4 visualises the different phases in the generation of a typical AP. In this context, the membrane potential is initially at rest (step 1). At some point, an electrode injects positive current in the soma which results in an increase (or depolarization) of the potential (step 2). If the potential exceeds

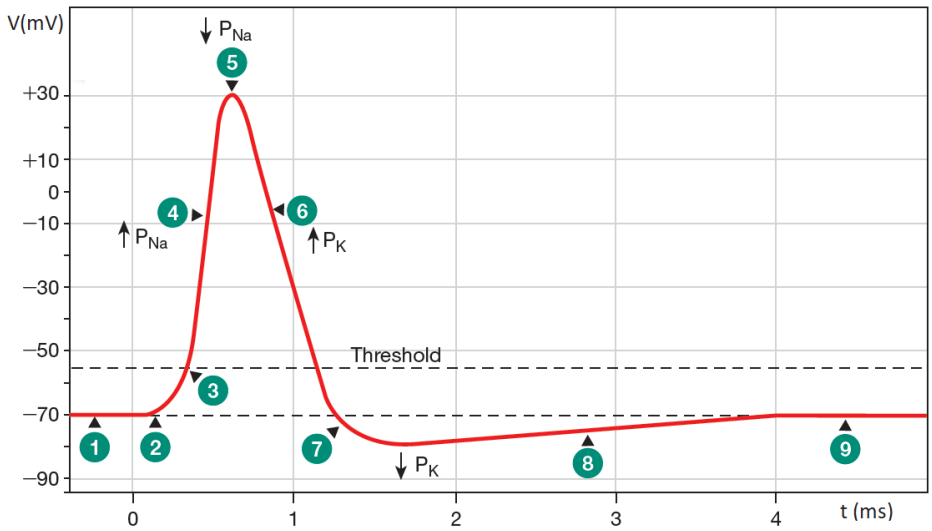

Figure 2.4: Generation of the Action Potential in steps. Taken from [10].

a threshold, then an AP will be formed, because voltage gated channels are coming into play (step 3), relatively independent of stimuli. Na^+ gates respond quicker than K^+ thus, Na^+ current enters the cell depolarizing further the membrane (step 4). The peak of the spike is reached as Na^+ channels close after a certain potential while more and more potassium channels open (step 5). The membrane is now more permeable to potassium current pushing the voltage closer to K^+ resting potential (step 6) which is lower than the membranes equilibrium (hyperpolarization). Finally, slower potassium channels also close and the voltage reaches the equilibrium (step 8 and 9).

At this point we need to provide some clarifications: first of all, the threshold is a confusing concept because almost in all occasions it is not a single value of the potential which acts as a threshold but a set of potential and conductance values, while in other cases a threshold is undefined [9]. Secondly, channels open and close in a way which ensures that during the time between steps 3-7, called absolute refractory period, it is impossible for the neuron to generate a second AP. On the other hand, in the time interval between steps 7-8, called relative refractory period, the generation of a second AP is possible, but relative stronger stimulus is needed.

2.3 Hodgkin - Huxley model

In the 1952 Hodgkin and Huxley created a model to explain the generation of APs on the squid giant axon. The HH model consists of a system of four first order, ordinary differential equations [9]. The first equation relates the potential of the membrane with 3 ionic currents: I_{Na^+}, I_{K^+} and an Ohmic leak current I_L. The former 2 currents are nonlinearly voltage dependent through gating variables n for I_{K^+} and m, h for I_{Na^+}:

$$\begin{aligned} C\dot{V} &= I - \bar{g}_K n^4 (V - E_K) - \bar{g}_{Na} m^3 h (V - E_{Na}) - \bar{g_L}(V - E_L) \\ \dot{n} &= a_n(V)(1-n) - \beta_n(V) n \\ \dot{m} &= a_m(V)(1-m) - \beta_m(V) m \\ \dot{h} &= a_h(V)(1-h) - \beta_h(V) h, \end{aligned} \tag{2.4}$$

where C is the membrane's capacitance, $\bar{g}_K$ and $\bar{g}_{Na}$ is the maximal conductance for each ion and the nonlinear functions a,β are:

$$\begin{aligned} a_n(V) &= 0.01 \frac{10 - V}{e^{\frac{10-V}{10}} - 1} \quad & \beta_n(V) &= 0.125 e^{\frac{-V}{80}} \\ a_m(V) &= 0.1 \frac{25 - V}{e^{\frac{25-V}{10}} - 1} \quad & \beta_m(V) &= 4 e^{\frac{-V}{18}} \\ a_h(V) &= 0.07 e^{\frac{-V}{20}} \quad & \beta_h(V) &= \frac{1}{e^{\frac{30-V}{10}} + 1}. \end{aligned} \tag{2.5}$$

Chapter 3

Dynamical Background

3.1 Dynamical Systems

A dynamical system consists of a set of variables that describe its state and a law that describes the evolution of these variables with time [9]. Mathematically, these systems are determined by differential or by difference equations (iterated maps). In this thesis, however, we are interested with the former case which can always be rewritten as a system of first order differential equations:

$$\begin{aligned} \frac{dx_1}{dt} &= f_1(x_1, ..., x_N) \\ &\vdots \\ \frac{dx_N}{dt} &= f_N(x_1, ..., x_N). \end{aligned} \tag{3.1}$$

For example a pendulum with mass m, damping coefficient b, length L and torque τ which obeys the relation:

$$mL^2\frac{d^2\theta}{dt^2} + b\frac{d\theta}{dt} + mgL\sin\theta = \tau,$$

can be rewritten as:

$$\begin{aligned} \frac{d\theta}{dt} &= \omega \\ \frac{d\omega}{dt} &= -\frac{b}{mL^2}\omega - \frac{g}{L}sin\theta + \frac{\tau}{mL^2}. \end{aligned} \tag{3.2}$$

A system is called nonlinear when it contains nonlinear terms of the variables (in this case $\sin\theta$). Generally, it is impossible to solve nonlinear systems analytically, however important qualitative information, for example the existence of oscillatory or resting solutions, can be extracted from the system through geometric methods [11].

A useful tool in this approach is an abstract space whose coordinates are the variables of the system (θ, ω) called phase space. As phase space of system (3.2) is composed of two variables, it is 2-dimensional. This system can be solved numerically, provided initial conditions $\theta(t = 0)$ and $\omega(t = 0)$ are given, hence we can calculate the timeseries $\theta(t)$ and $\omega(t)$. Solution $(\theta(t), \omega(t))$ represents a curve on the phase plane and is called a trajectory. Note that for "normal" systems two trajectories can never intersect because there would exist two different solutions with the same initial conditions, which is forbidden from the Existence and Uniqueness Theorem [11].

System (3.1) can be written in a more compact form:

$$\frac{d\vec{x}}{dt} = \vec{f}(\vec{x}), \tag{3.3}$$

where $\frac{d\vec{x}}{dt}$ represents the vector field which can be sketched on the phase plane as in Fig. 3.1. A trajectory is always tangent to the vector field.

3.2 Linear Systems

We now present briefly the theory of linear systems as it will be used with some alterations in the nonlinear case. The most general form of a linear system is:

$$\frac{d\vec{x}}{dt} = \boldsymbol{A}\vec{x}, \tag{3.4}$$

where $\boldsymbol{A}$ is the matrix of coefficients with N dimensions. We search for solutions of the form:

$$\frac{d\vec{v}}{dt} = e^{\lambda t}\vec{v}, \tag{3.5}$$

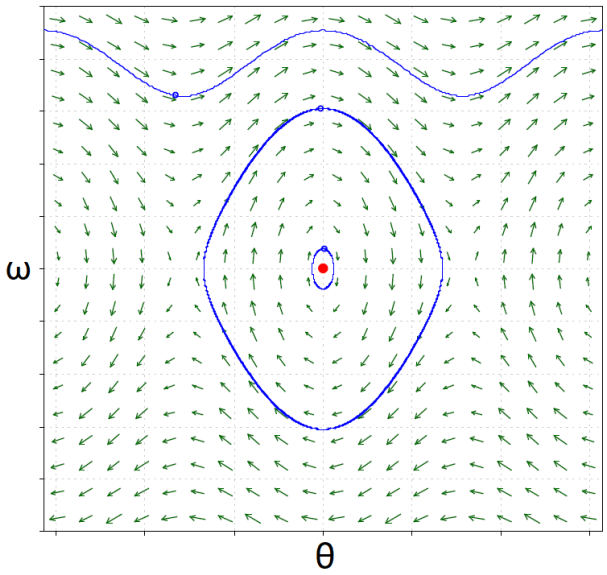

Figure 3.1: Vector field for the pendulum. Blue curves are oscillatory trajectories while the red dot is the equilibrium. Parameters: $b = 0$, $m = 1$, $L = 1$, $g = 9.8$, $\tau = 0$.

because they are generalizations of the 1-dimensional case. Combining (3.4), (3.5) gives:

$$e^{\lambda t}\vec{v} = \boldsymbol{A}\vec{v}, \tag{3.6}$$

which is known as the eigenvalue problem. Supposing $\boldsymbol{A}$ is non degenerate, we can find $\lambda_i, \vec{v_i}$ where i = 1,2,..,N. Then, the complete solution of (3.4) is:

$$\vec{x}(t) = c_1 e^{\lambda_1 t}\vec{v}_1 + ... + c_N e^{\lambda_N t}\vec{v}_N. \tag{3.7}$$

The coefficients c_i are calculated from the initial conditions. The eigenvectors show the "important" directions of the system while the eigenvalues explain its behaviour. To gain more insight we now solve a general 2-dimensional problem described by the following matrix:

$$\boldsymbol{A} = \begin{bmatrix} a & b \\ c & d \end{bmatrix}.$$

The system has one fixed point ($\frac{d\vec{x}}{dt} = 0$) which is the origin. $\boldsymbol{A}$ has trace

$\tau = a + d$, determinant $\Delta = ad - bc$ and eigenvalues:

$$\lambda_{1,2} = \frac{\tau \pm \sqrt{\tau^2 - 4\Delta}}{2}. \tag{3.8}$$

From (3.7) and (3.8) we derive the behaviour of the system depending on the eigenvalues:

- For real, negative eigenvalues the fixed point is called stable node because all trajectories will converge to it exponentially.
- For real, positive eigenvalues the fixed point is called unstable node because all trajectories will diverge exponentially from it.
- For real eigenvalues with opposite sign the fixed point is called saddle node. Most trajectories will approach the saddle node but eventually all of them will diverge exponentially from it.
- For complex eigenvalues with negative real part the fixed point is called stable focus because all trajectories will converge in an oscillatory manner.
- For complex eigenvalues with positive real part the fixed point is called unstable focus because all trajectories will diverge in an oscillatory manner.
- For imaginary eigenvalues (zero real part) the fixed point is called neutrally stable equilibrium or center. All trajectories are periodic, forming a continuum of infinitesimally closed orbits.

Note that all possible behaviours are simple. The fixed point (also equilibriun) can be stable with all trajectories being attracted by it, unstable with all trajectories being repelled from it and neutrally stable. Conventionally, we represent the first case with a solid black dot and the second case with an open circle.

Figure 3.2 collects all these behaviours. The borderlines between different areas, centers included, are exceptional cases which will not be discussed more as they are not useful for nonlinear systems. For higher dimensional systems we can not use Fig. 3.2 but we can still derive the behaviour of an equilibrium from its eigenvalues and identify it accordingly. For example, in a 3-dimensional system a fixed point with two complex eigenvalues of negative real part and one real positive eigenvalue is called saddle-focus.

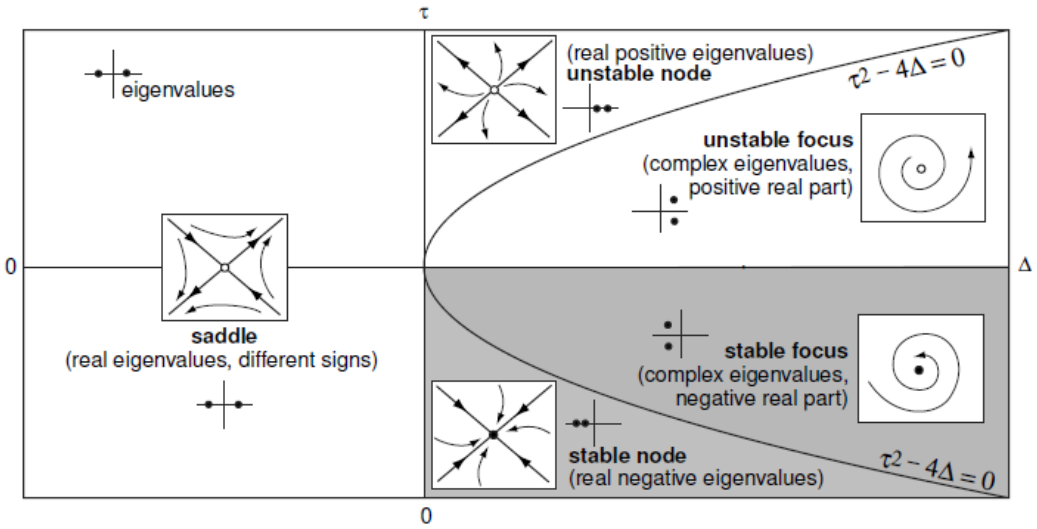

Figure 3.2: Summary of all important behaviours of a 2-dimensional linear system. Grey area denotes the stable regime. Taken from [9].

3.3 Nonlinear systems

We now present briefly some new characteristics of nonlinear systems and the tools which are used in order to analyze them.

3.3.1 Equilibria

Equilibria can be found in two consecutive steps. Firstly, we compute $f_i(x_1, .., x_N) = 0$ from equation (3.3) which provides N curves, called nullclines. These curves are very helpful for qualitative comprehension of the system as will be shown below. After that, the equilibria are found at the intersections of the nullclines. The stability of the fixed points is calculated by taking a linear approximation of the nonlinear system infinitesimally close to the fixed point [11]. Practically, that means we need to compute the Jacobian at the fixed point $\vec{x}^\star$:

$$\boldsymbol{J}_{\vec{x}^\star} = \begin{bmatrix} \frac{\partial f_1}{\partial x_1} & \cdots & \frac{\partial f_1}{\partial x_N} \\ \vdots & \ddots & \vdots \\ \frac{\partial f_N}{\partial x_1} & \cdots & \frac{\partial f_N}{\partial x_N} \end{bmatrix}_{\vec{x}^\star} . \tag{3.9}$$

Then, we need to follow the procedure explained above for the linear

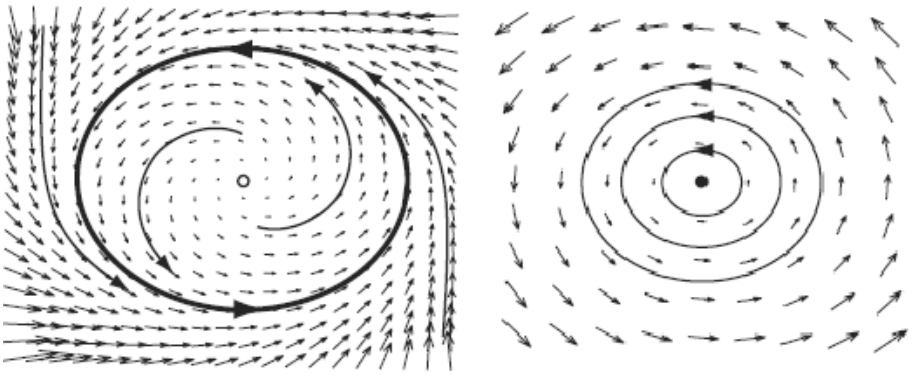

Figure 3.3: Stable limit cycle vs center. Taken from [9].

system. This algorithm will not produce reliable results for the borderline cases of Fig. 3.2 because small nonlinear terms which are not taken into account by the Jacobian are essential. Of all cases that have been mentioned so far only centers are of that type.

3.3.2 Limit Cycles

A new behaviour which does not exist in linear systems is isolated periodic trajectories called limit cycles (LC). In the case of a LC, trajectories in its vicinity will converge to an oscillation (stable LC) or diverge from one (unstable LC). In contrast, oscillatory behaviours in linear systems are exceptional cases (all eigenvalues must be imaginary) where all trajectories are eclipses on the phase plane and are infinitesimally close to each other. Conventionally, unstable LCs are represented with a solid curve and unstable LCs by a dashed curve.

3.3.3 Chaos

Chaotic behaviour can exist in nonlinear systems with more than two dimensions. It is difficult to define chaos, though, the following three properties should meet simultaneously [11].

- Aperiodic long term behaviour: There should be an open set of initial conditions leading to aperiodic trajectories which do not settle down to fixed points.

- Deterministic: The system's behaviour arises from nonlinear terms, not due to stochasticity.
- Sensitive dependence on initial conditions: Nearby trajectories separate exponentially fast.

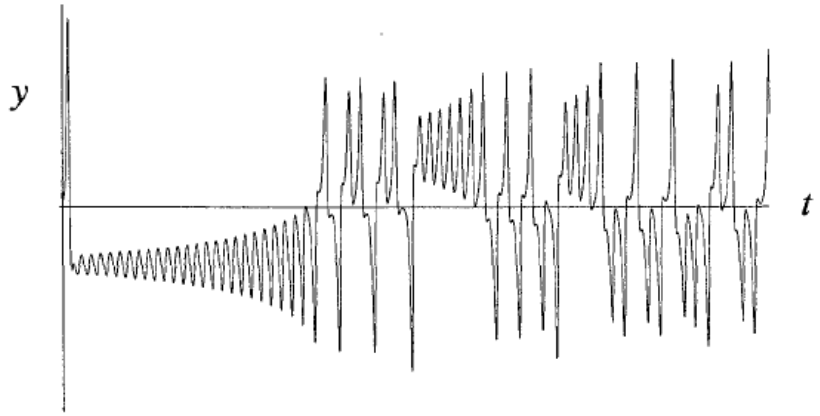

Figure 3.4: Chaotic behaviour in Lorenz system. Variable y does not settle down or converge to periodic movement.

The third property provides a tool to analyze chaos, namely the Lyapunov exponents. Suppose we follow two trajectories which are initially very close, separated by a very small vector $\vec{\delta_0}$ in the phase plane. While they evolve we keep track of their difference $\vec{\delta}(t) = \vec{x}_1(t) - \vec{x}_0(t)$. In a chaotic system $\vec{\delta}(t)$ can be approximated for some finite time by:

$$|\vec{\delta}(t)| = |\vec{\delta_0}|e^{\Lambda t}. \tag{3.10}$$

The approximation can not hold forever because the trajectories are confined in a finite volume of the phase plane, thus at some point $\vec{\delta}(t)$ will be stabilized. From equation (3.10) we calculate the maximum Lyapunov exponent Λ. This concept can be generalized for N different exponents in an N-dimensional system. We now follow an infinitesimal sphere of initial conditions which distorts as the system evolves. Following the procedure explained above for each axis of the sphere we calculate N exponents.

Lyapunov exponents provide useful information about a system [12]. First of all, the time-average of the divergence of the system $\vec{\nabla}\vec{f}$ is equal to their sum. Thus, we can understand whether the system is dissipative, when

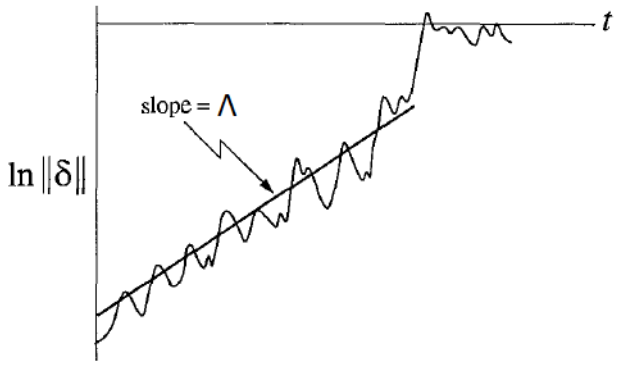

Figure 3.5: Calculation of maximum exponent in Lorenz system. Taken from [11].

the sign of their sum is negative, or conservative, when their sum is zero. Furthermore, if a system rests, all Lyapunov exponents must be negative, while in the case of a stable LC, the maximum exponent is zero. Finally, chaos in dissipative systems corresponds to at least one positive exponent.

3.3.4 Bifurcations

A dynamical system's behaviour can change dramatically as its parameters are varied. A typical biological example is that neurons are producing APs when receiving appropriate stimuli whereas, in any other case, they rest. These transitions are called bifurcations. We now present the main bifurcations in neuronal systems which can be split in two categories.

Bifurcations of fixed points

They are discovered analytically relatively easy. For each bifurcation, we present a single example along with the necessary condition which we use to discover it.

- Saddle-Node (SN) bifurcation. A stable and an unstable fixed point are getting closer as the bifurcation parameters varies. At some point they collide resulting in their disappearance. At bifurcation point one eigenvalue for each fixed point is zero. All SN bifurcations can be reduced to the 1-dimensional system:

$$\frac{dx}{dt} = f(x, r) = x^2 - \mu. \tag{3.11}$$

- Saddle-Node on Invariant Circle (SNIC) bifurcation. This is a SN with the additional condition that two trajectories connect the unstable with the stable fixed point. Thus, when they disappear a LC appears. A simple example in polar coordinates is:

$$\begin{aligned} \frac{dr}{dt} &= r(1-r^2) \\ \frac{d\theta}{dt} &= \mu - sin\theta. \end{aligned} \tag{3.12}$$

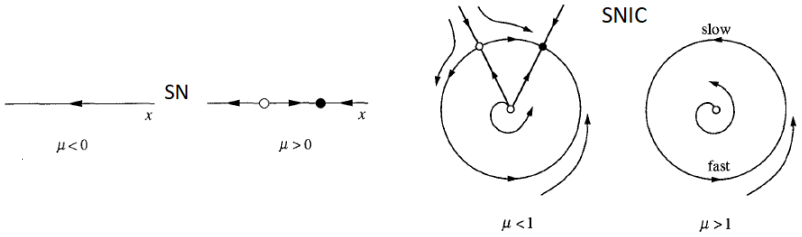

Figure 3.6: Bifurcations for simple systems (3.11) and (3.12). Taken from [11].

In both SN and SNIC bifurcations two fixed points (dis)appear as a parameter varies. On the contrary, during a Hopf bifurcation a focus changes stability as it crosses the border $\Delta = 0$ of Fig. 3.2 with the help of a LC. At the bifurcation point the real part of the eigenvalues of a focus is zero. There are two types of Hopf bifurcations:

- Superctitical Hopf bifurcation. In this case a stable focus is transformed into an unstable one while a stable LC is born. A simple system with this behaviour is:

$$\begin{aligned} \frac{dr}{dt} &= \mu r - r^3 \\ \frac{d\theta}{dt} &= \omega + r^2. \end{aligned} \tag{3.13}$$

- Subcritical Hopf bifurcation. In this case an unstable LC falls into a stable focus transforming it into an unstable focus. A simple example is:

$$\begin{aligned} \frac{dr}{dt} &= \mu r + r^3 - r^5 \\ \frac{d\theta}{dt} &= \omega + r^2. \end{aligned} \tag{3.14}$$

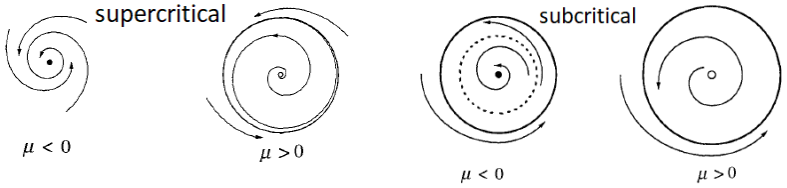

Figure 3.7: Bifurcations for simple systems (3.13) and (3.14) . Taken from [11].

In both (3.13) and (3.14) systems μ is the bifurcation parameter and ω is the angular frequency.

Bifurcation of Limit Cycles

We have already seen bifurcations were a LC participates (Hopf, SNIC) though, they can always be discovered from the conditions of their fixed points. The bifurcations we are going to present now, in contrast, are more difficult to examine analytically. We omit conditions and examples and present the bifurcations in a more geometrical way.

- Fold Limit Cycle (FLC) bifurcation. It is the equivalent of SN for cycles. An unstable cycle collides with a stable one resulting in their disappearance.

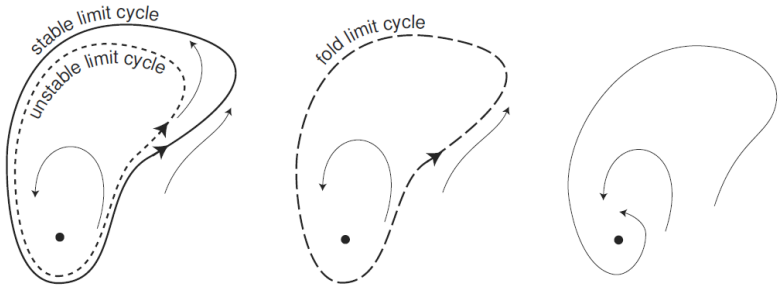

Figure 3.8: Fold Limit Cycle bifurcation. Taken from [9].

- Supercritical (Subcritical) Homoclinic bifurcation. A saddle node is near a stable (unstable) LC. While the bifurcation parameter is varied, the LC gets closer to the SN until it touches it. At this point, the LC becomes a homoclinic trajectory because it starts from and ends at the saddle node (though it takes infinite time). Then, the LC disappears. We can distinguish the subcritical from the supercritical case, with the

latter being more common in neuronal models, from the saddle quantity σ. It is defined as the sum of the smaller positive real part and the larger negative real part of the eigenvalues [13]. If $\sigma < 0 (> 0)$ at the bifurcation point, the bifurcation is supercritical (subcritical).

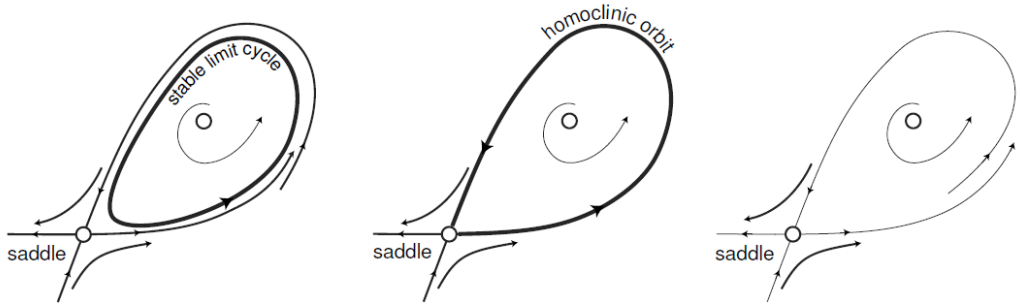

a. supercritical saddle homoclinic orbit bifurcation

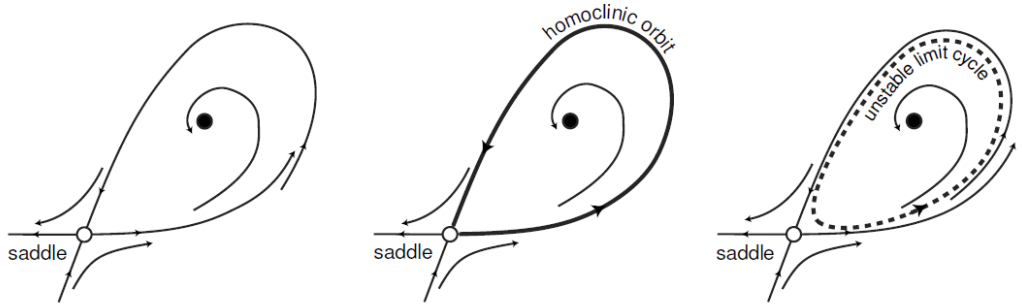

b. subcritical saddle homoclinic orbit bifurcation

Figure 3.9: Homoclinic bifurcation. Taken from [9].

Some times bifurcations are detected through characteristic relations between the amplitude and period of the involved stable LC and the bifurcation parameter, called scaling laws. This is extremely helpful in the cases where analytical computation is difficult.

A bifurcation diagram summarizes the different behaviours of a system near a bifurcation point. In it, we plot the bifurcation parameter with a variable of the system. For equilibria the relation between variable and bifurcation parameter is 1-1 while for cycles we need to pick one value from the limit cycle, for example the maximum.

	Amplitude of LC	Period of LC
Supercritical Hopf	$O(\sqrt{\mu})$	$O(1)$
SN of cycles	$O(1)$	$O(1)$
SNIC	$O(1)$	$O(\frac{1}{\sqrt{\mu}})$
Homoclinic	$O(1)$	$O(\ln \mu)$

Table 3.1: Table of important scaling laws. Taken from [11].

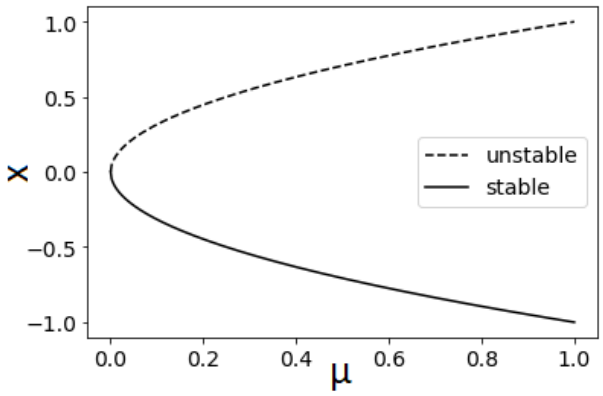

Figure 3.10: One-dimensional bifurcation diagram of system (3.11).

Codimension-2 bifurcations

All bifurcations examined until now occur through tuning one parameter. That is why they are called codimension-1 bifurcations. In this study we will also come across a codimension-2 bifurcation, namely a Saddle-Node Loop (or Saddle-Node Homoclinic Orbit bifurcation). In this scenario, a saddle node is between a fixed point and a LC, for some parameter values (grey part of Fig. 3.11). Moving across a direction in the parameter space brings the stable equilibria closer to the saddle node until they annihilate through a SN bifurcation. In the opposite direction, the LC gets closer to the saddle node until it disappears via a Homoclinic bifurcation. These two bifurcations occur more and more closer as we approach the codimension-2 bifurcation point until they coalesce in order to form a SNIC bifurcation.

We can collect all different behaviours near the SNL bifurcation over the parameter space in a stability diagram shown in Fig. 3.11. The curves in this diagram correspond to bifurcation lines and, therefore, their intersection marks the codimension-2 bifurcation point. There, all three bifurcation lines "collide".

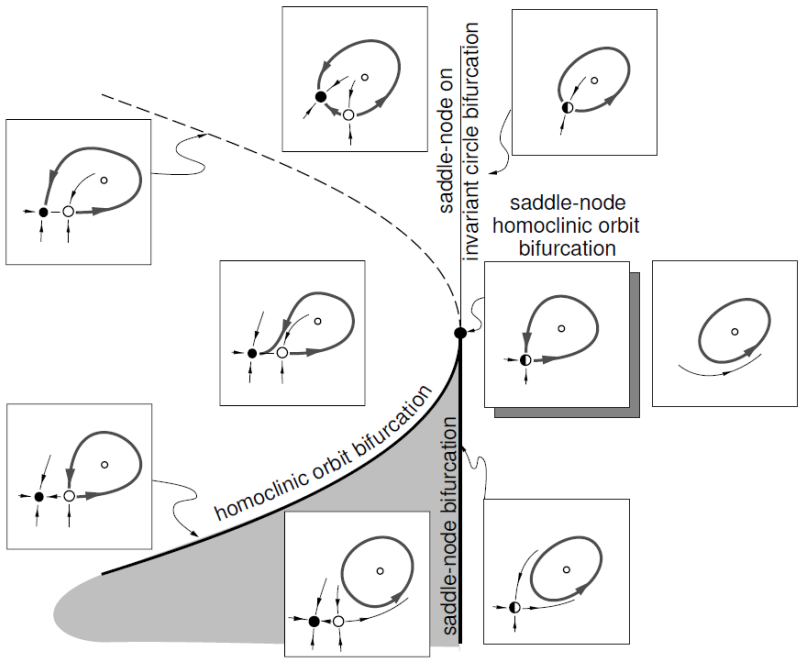

Figure 3.11: The general form of a SNL bifurcation. Taken from [9].

3.4 Neurons as Dynamical Systems

The HH model (2.4) shows that neurocomputational concepts can be analyzed within the framework of dynamical systems. Neuronal behaviour, like quiescence, correspond to a dynamical behaviour of the model, like a global equilibrium, while a change in the behaviour corresponds to a bifurcation. In the HH model for example, the current I is a bifurcation parameter. In this section, we present some important properties of neurons along with their equivalent dynamics, following [9].

Before starting, we can reduce the HH model to a 2-dimensional one, making the presentation of new concepts easier. Assuming that the gating variables for Na are much faster than the others, we obtain the persistent sodium plus potassium model $I_{Na,p} + I_K$ which has two variables, V and n.

Hodgkin Classification

Historically, one possible categorization of neurons is done according to the frequency of the APs in response to the applied current (F-I curve).

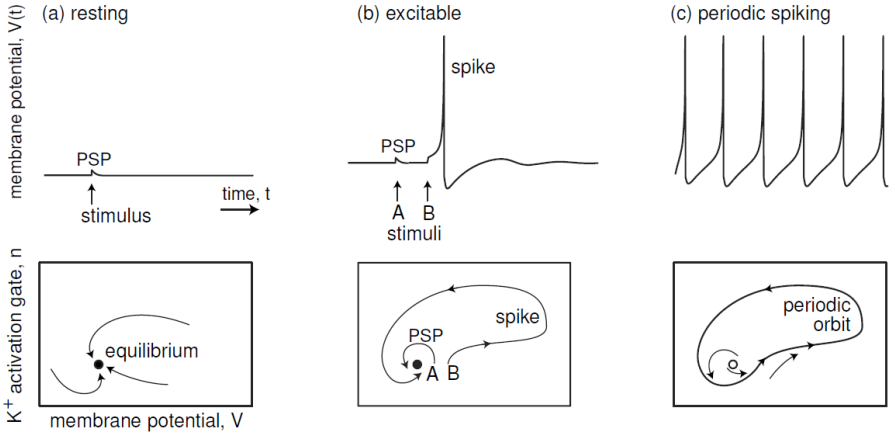

Figure 3.12: Top: Neuron-like responses. Bottom: Phase planes. PSP stands for postsynaptic potential. Taken from [9].

- Class 1 neural excitability: Spikes can be generated with arbitrarily low frequency. The transition "resting" $\rightarrow$ "spiking" occurs through a SNIC bifurcation, because it is the only bifurcation of fixed points with a continuous scaling law for the frequency (see Table 3.1).

- Class 2 neural excitability: Spikes cannot be generated with arbitrarily low frequency, and there is a discontinuity in the F-I curve. This transition can occur through a SN, a subcritical Hopf or a supercritical Hopf bifurcation.

Bistability

Bistable neurons are able to rest or spike spike depending on their initial conditions. Dynamically, coexistence of stable fixed points and a stable LC can occur before a SN or a subcritical Hopf bifurcation. Bistability coincides with a hysteresis loop in the F-I diagram. Note that the transition "resting" $\rightarrow$ "spiking" occurs via a different mechanism than the transition "spiking" $\rightarrow$ "resting". We can define the Hodgkin classification of neural spiking, similarly to the classification of neural excitability, where we take into account the latter transition.

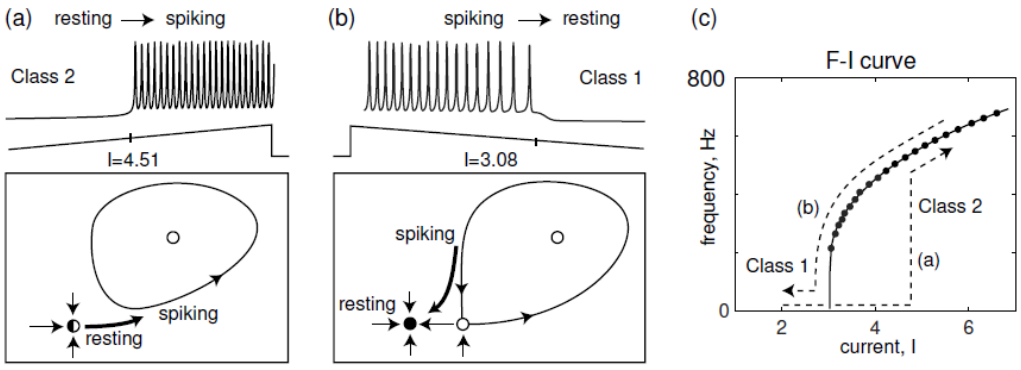

Figure 3.13: Bistability before a SN bifurcation. Spiking stops via a homoclinic bifurcation. Taken from [9].

Resonators vs Integrators

A neuron which exhibits subthreshold damped oscillations is called a resonator, while when it lacks this property it is called an integrator. In 2 dimensions, resonators correspond to systems near a Hopf bifurcation while integrators undergo SNIC or SN bifurcations. Both categories are linked with distinct neurocomputational properties, summarized in Table 3.2.

properties	integrators	resonators
Subthreshold oscillations	no	yes
Bifurcation	SNIC or SN	sub/supercritical Hopf
Bistability	possible	possible
Frequency preference	no	yes
Spike latency	large	small
Threshold	well defined	may not be defined
Post-inhibitory spike	no	yes
Inhibition induced spiking	no	possible

Table 3.2: Summary of neurocomputational properties for integrators and resonators in 2-dimensional models. Taken from [9].

In more dimensions there could be alterations in the table, for example a 3-dimensional system can undergo a SN bifurcation while exhibiting subthreshold damped oscillations.

Some properties of Table 3.2 may be unfamiliar. We briefly explain them now.

- Spike latency refers to the ability of some neurons to generate a spike with considerable delay, in response to a barely superthreshold stimulus.
- Post-inhibitory spikes are APs generated from neurons, which have been hyperpolarized by some negative current, when this current goes off.
- Inhibition induced spiking are APs generated from neurons in response to sustained hyperpolarization.

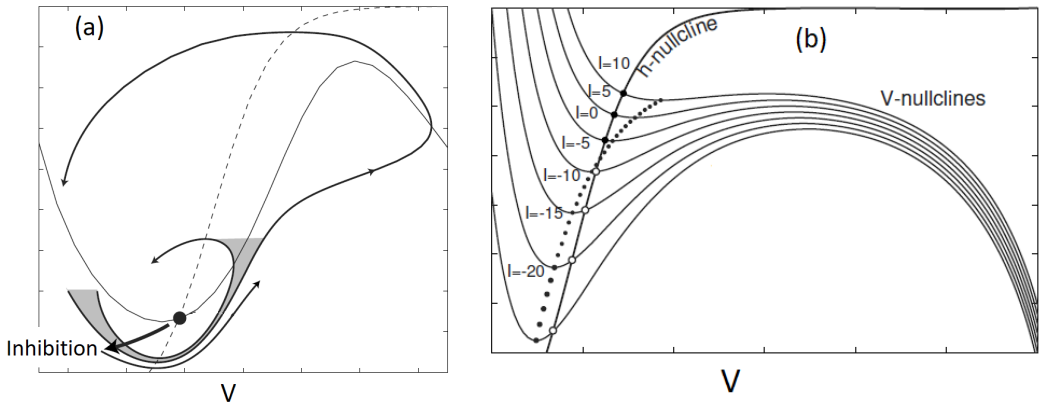

Figure 3.14: (a) Post-inhibitory spikes. Brief hyperpolarization pushes the system to follow a spiking trajectory in order to find its resting point. (b) Inhibition induced spiking. Sustained hyperpolarization transforms a stable to an unstable fixed point. As long as hyperpolarization stands, the neuron is spiking. Taken from [9].

Chapter 4

Josephson Junction Neurons

As mentioned in the introduction, one way to emulate neuronal behaviour is by using Josephson junctions (JJ). In the following section the physics of JJs is briefly presented.

4.1 Josephson Junctions

A Josephson junction is made up of two superconductors coupled by a weak link, such as, a thin insulator [11]. The wave functions $\psi_1 e^{i\phi_1}$ and $\psi_2 e^{i\phi_2}$ describe the ground state of the electrons in the two superconducting areas. Solving the Schrödinger equation for the system, yields that both current and voltage are functions of the phase difference $\phi = \phi_1 - \phi_2$. More specifically, the Josephson current-phase relation is:

$$I = I_{cr} \sin \phi, \tag{4.1}$$

where I_{cr} is called the critical current. Furthermore, the Josephson voltage-phase relation reads:

$$V = \frac{\hbar}{2e} \frac{d\phi}{dt}. \tag{4.2}$$

The remarkable property of the junction is that, theoretically, smaller currents than the critical one can pass through, without any voltage across it, corresponding to a junction with zero resistance!

In reality, in addition to the supercurrent of Eq. (4.1), there are contributions from displacement and ordinary currents, which can be modelled by

a capacitor with capacitance C and a resistor with resistance R respectively. In this way, the equivalent circuit of a JJ is obtained, which is shown in Fig. 4.1.

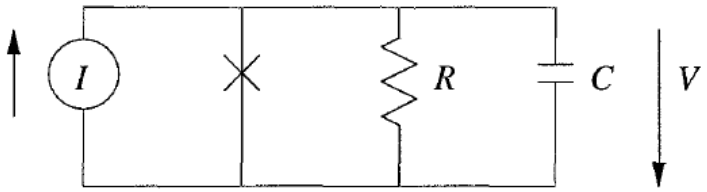

Figure 4.1: Equivalent JJ circuit. Taken from [11].

Using the second law of Kirchhoff we derive:

$$C\frac{dV}{dt} + \frac{V}{R} + I_{cr}\sin\phi = I. \tag{4.3}$$

Substituting (4.2) in (4.3) we obtain:

$$\frac{\hbar C}{2e}\frac{d^2\phi}{dt} + \frac{\hbar}{2eR}\frac{d\phi}{dt} + I_{cr}\sin\phi = I. \tag{4.4}$$

Remarkably, Eq. (4.4) is the electrical analog of a damped pendulum driven by constant torque, which was introduced in Chapter 2.

The first step in order to solve the system is to normalize the time scale, the current and the damping coefficient according to:

$$\bar{t} = \sqrt{\frac{2eI_{cr}}{\hbar C}}t, \quad i = \frac{I}{I_{cr}}, \quad \Gamma = \sqrt{\frac{\hbar}{2eI_{cr}R^2C}}, \tag{4.5}$$

which simplifies the Eq. (4.4) to the non-dimensional form:

$$\frac{d^2\phi}{d\bar{t}^2} + \Gamma\frac{d\phi}{d\bar{t}} + \sin\phi = i. \tag{4.6}$$

When a constant current is running trough a JJ, two different behaviours are possible, which can be pictured with the help of the mechanical analog. Depending on the parameters (and the initial conditions in the case of bistability), the body can either stay still, when the torque and the gravity are balanced, or rotate, when the torque overcomes gravity.

The dynamics of the system are summarized in the stability diagram of Fig. 4.2. Note that the system undergoes a SNL bifurcation because its stability diagram is the same with Fig. 3.11, if we swap the axes.

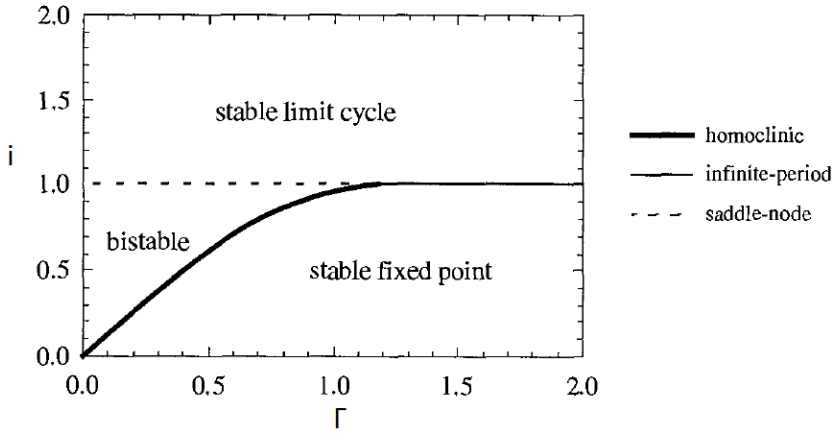

Figure 4.2: Stability diagram. Adapted from [11].

4.2 JJ Neuron

Two JJs coupled together can model a biological neuron with each junction emulating an ionic channel [6]. The neuromorphic circuit is presented in Fig. 4.3. The two JJs are called pulse (p) and control (c) and, in this thesis, they are always considered as identical. The current I_{in} emulates the stimulus provided from another neuron (or a neuroscientist). The current I_b provides the necessary amount of energy to the JJs for spikes to be generated and it is assumed constant.

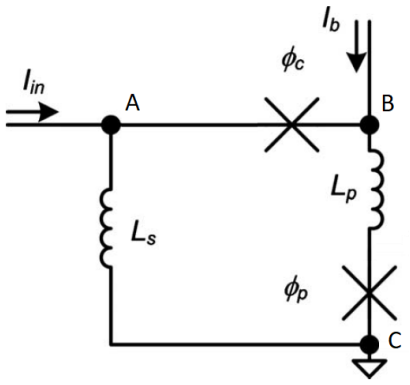

Figure 4.3: Circuit which acts like a neuron. Adapted from [6].

Using Kirchhoff's laws, we derive the equations which describe the system. Currents are denoted by I, where subscripts "p", "c" and "s" specifie the electrical element through which the respective current is flowing. The same

applies for the voltage differences.

Kirchhoff's current law for nodes A and B yields:

$$\begin{cases} I_c + I_b = I_p \\ I_{in} = I_c + I_s \end{cases} \implies I_s = I_{in} - I_p + I_b. \tag{4.7}$$

Kirchoff's voltage law for the circuit is:

$$\begin{cases} V_B - V_C = V_{Lp} + V_{JJp} \underset{V_C=0}{\implies} V_{Lp} = V_B - V_{JJp} \\ V_B - V_C = -V_{JJc} + V_s \implies V_B = -V_{JJc} + V_s \end{cases}$$

$$\implies V_{Lp} = -V_{JJc} + V_S - V_{JJp}. \tag{4.8}$$

We now substitute the voltage difference across a junction using Eq. (4.2) and across an inductor with $V = L\frac{dI}{dt}$:

$$L_p \frac{dI_p}{dt} = -\frac{\hbar}{2e}\frac{d\phi_p}{dt} - \frac{\hbar}{2e}\frac{d\phi_c}{dt} + L_s \frac{dI_s}{dt}. \tag{4.9}$$

Integrating over time in the interval $[0, t]$ yields:

$$L_p I_p = -\frac{\hbar}{2e}(\phi_p + \phi_c) + L_s I_s \overset{(4.7)}{\implies} L_p I_p = -\frac{\hbar}{2e}(\phi_p + \phi_c) + L_s(I_{in} - I_p + I_b). \tag{4.10}$$

Now Eq. (4.10) needs to be normalized.

Currents I_c, I_p, I_{in}, I_b are normalized with respect to the critical current of the junctions I_{cr}, becoming i_c, i_p, i_{in}, i_b respectively.

We also normalize inductances by:

$$\Lambda_s = \frac{L_s}{L_s + L_p}, \quad \Lambda_p = \frac{L_p}{L_s + L_p}. \tag{4.11}$$

Then, the coupling coefficient is:

$$\lambda = \frac{\hbar}{2e(L_s + L_p)I_{cr}}. \tag{4.12}$$

Solving for i_p, we find:

$$i_p = -\lambda(\phi_p + \phi_c) + \Lambda_s i_{in} + (1 - \Lambda_p) i_b. \tag{4.13}$$

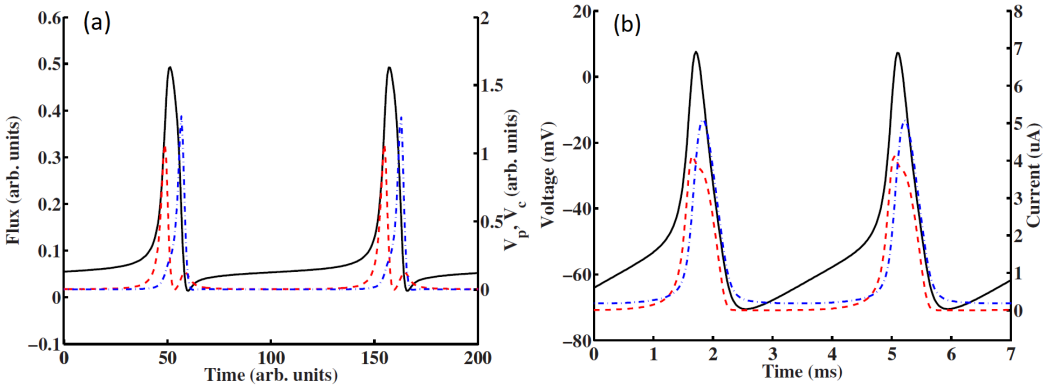

Figure 4.4: Comparison between a JJ neuron (a) and a HH (b) neuron when both are forced to spike repetitively. Solid black lines depict the magnetic flux and membrane potential, respectively. Red dashed lines depict the voltage ($\dot{\phi_p}$) across the pulse junction and the Na^+ current. Blue dot-dashed lines depict the absolute value voltage (-$\dot{\phi_c}$) across the control junction and the absolute value of K^+ current. Taken from [6].

The current conservation law yields:

$$i_c = -\lambda(\phi_p + \phi_c) + \Lambda_s i_{in} - \Lambda_p i_b. \tag{4.14}$$

Combining Eqs. (4.13), (4.14) and (4.6) we finally have:

$$\begin{aligned} \ddot{\phi_p} + \Gamma\dot{\phi_p} + \sin\phi_p &= -\lambda(\phi_p + \phi_c) + \Lambda_s i_{in} + (1 - \Lambda_p) i_b, \\ \ddot{\phi_c} + \Gamma\dot{\phi_c} + \sin\phi_c &= -\lambda(\phi_p + \phi_c) + \Lambda_s i_{in} - \Lambda_p i_b, \end{aligned} \tag{4.15}$$

where the dot refers to the derivative with respect to the dimensionless time $\bar{t}$ of relation (4.5).

The magnetic flux $\lambda(\phi_p + \phi_c)$ of the circuit is the equivalent of the membrane potential. In the appendix A, we visualise the generation of the APs with the help of the mechanical analog. Here we just highlight that voltages across the pulse and the control junction act like the Na^+ and K^+ currents, respectively. More specifically, during the early stages of the generation of an AP, $\dot{\phi_p}$ forces the flux to grow rapidly, until a certain point, where $\dot{\phi_p}$ becomes negligible. On the contrary, $\dot{\phi_c}$, which becomes important at a later point, reduces the flux resulting in the downstroke of the spike. At this stage, the generation of a new spike is extremely difficult resulting in a refractory period-like behaviour.

Chapter 5

Mathematical Analysis

5.1 Linear stability analysis

The initial system is governed by the following equations:

$$\ddot{\phi}_p + \Gamma\dot{\phi}_p + \sin\phi_p = -\lambda(\phi_c + \phi_p) + \Lambda_s i_{in} + (1-\Lambda_p)i_b \tag{5.1}$$
$$\ddot{\phi}_c + \Gamma\dot{\phi}_c + \sin\phi_c = -\lambda(\phi_c + \phi_p) + \Lambda_s i_{in} - \Lambda_p i_b. \tag{5.2}$$

We define $\dot{\phi}_p = \omega_p$ and $\dot{\phi}_c = \omega_c$. Then, the system becomes:

$$\dot{\phi}_p = \omega_p \tag{5.3}$$
$$\dot{\omega}_p = -\Gamma\omega - \sin\phi_p - \lambda(\phi_c + \phi_p) + \Lambda_s i_{in} + (1-\Lambda_p)i_b \tag{5.4}$$
$$\dot{\phi}_c = \omega_c \tag{5.5}$$
$$\dot{\omega}_c = -\Gamma\omega_c - \sin\phi_c - \lambda(\phi_c + \phi_p) + \Lambda_s i_{in} - \Lambda_p i_b, \tag{5.6}$$

with nullclines given by:

$$\omega_p = 0 \tag{5.7}$$
$$\phi_c = -\frac{\sin\phi_p}{\lambda} - \phi_p + \frac{\Lambda_s i_{in} + (1-\Lambda_p)i_b}{\lambda} \tag{5.8}$$
$$\omega_c = 0 \tag{5.9}$$
$$\phi_p = -\frac{\sin\phi_c}{\lambda} - \phi_c + \frac{\Lambda_s i_{in} - \Lambda_p i_b}{\lambda}. \tag{5.10}$$

In Fig. 5.1 we plot the nullclines (5.8) and (5.10) in the subspace $(\phi_p, 0, \phi_c, 0)$ of the phase space. In this way, many aspects of the model are qualitatively

understood. In principle, the two nullclines consist of an oscillatory part and a linear part, which has slope -1 and some intercept. The directions of the oscillations are perpendicular. Furthermore, the parameters modulate different behaviour of the nullclines. More specifically:

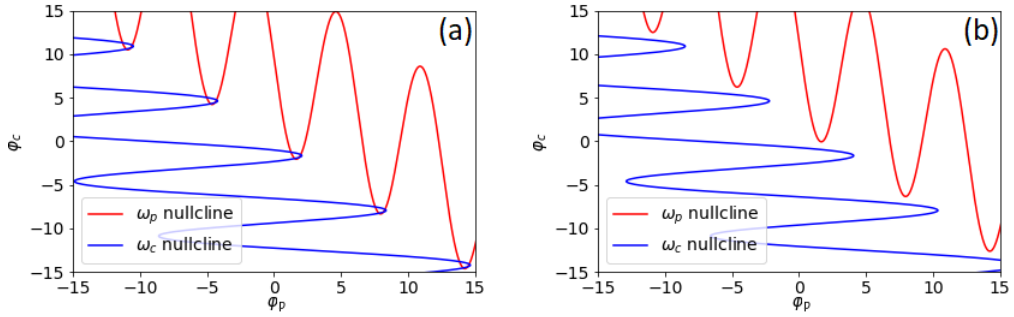

Figure 5.1: Nullclines $\dot{\omega_p} = 0$ and $\dot{\omega_c} = 0$ in the plane (ϕ_p, ϕ_c). The intersections of the nullclines correspond to fixed points. (a) For $i_{in} = 0$, the nullclines intersect periodically. (b) For $i_{in} = 0.4$, there are no equilibria. The other parameters: $\Lambda_p = 0.5$, $\Lambda_s = 0.5$, $\lambda = 0.1$ and $i_b = 1.909$ are kept fixed.

- Λ_s: It corresponds to the portion of i_{in} which passes through both JJs "c" and "p". In this thesis, we choose $\Lambda_s = 0.5$.

- Λ_p: This parameter is responsible for splitting i_b in two portions Λ_p and $1 - \Lambda_p$ which flow through junctions "c" and "p" respectively. We remind that $\Lambda_p \in (0, 1)$ and $\Lambda_p + \Lambda_s = 1$. Thus, $\Lambda_p = 0.5$ too.

- λ: Defines the amplitude of the oscillatory part and, furthermore, it is a scaling factor for the intercept of the linear part of the nullclines. In this thesis $\lambda = 0.1$.

- i_b: This current is essential in the generation of the spike, because it modulates the intercept of the linear part for each nullcline. Note that, the nullclines correspond to functions with different domains, namely, the domain for nullcline given by Eq. (5.8) is ϕ_p, while the domain for nullcline given by Eq. (5.10) is ϕ_c and that $(1 - \Lambda_p)i_b$ and $-\Lambda_p i_b$ have opposite sign. Subsequently, increasing i_b moves the ω_p nullcline upward and the ω_c nullcline leftward on the phase planes of Fig. 5.1.

Large absolute values of i_b result in the absence of equilibria because the nullclines never intersect, independently of the stimulus. The limit is calculated by subtracting Eqs. (5.8) and (5.10), yielding the relation: $\sin\phi_p - \sin\phi_c = i_b$. Thus, for $|i_b| > 2$ there are no equilibria. In the opposite case where $i_b = 0$, the nullclines are too intertwined and the system will never exhibit spikes, independently of the stimulus. In our case, there is a need of equilibria which disappear depending on the stimulus i_{in}. Therefore, $i_b = 1.909$ is used.

- i_{in}: As mentioned before, this current emulates the stimulus. Mathematically, the term $\Lambda_s i_{in}$ exists in both Eqs. (5.8) and (5.10). Increasing the current i_{in} moves the ω_p nullcline upward and the ω_c nullcline rightward. Figure 5.1 shows that this movement forces the nullclines to drift apart. Note that if i_{in} increases even more, the two nullclines will intersect again. In a JJ neuron, i_{in} constantly changes. Therefore, we need to study how these changes affect the neuronal behaviour.

- Γ: It does not affect the existence of the equilibria because it is not contained in the expressions of the nullclines. Nonetheless, Γ becomes important in the stability of the fixed points and in the birth and shape of the LCs. For this reason, this parameter is also studied.

We can quantitatively prove the aforementioned observations for i_{in} and i_b. Firstly, we need to calculate the positions of the equilibria by substituting Eq. (5.8) in Eq. (5.10). In this way, we get a relation which provides the $\phi_p^\star$ coordinate of the fixed points:

$$\sin\phi_p^\star - \sin\left(-\frac{\sin\phi_p^\star}{\lambda} - \phi_p^\star + \frac{\Lambda_s i_{in} + (1-\Lambda_p) i_b}{\lambda}\right) = i_b. \tag{5.11}$$

Then, the $\phi_c^\star$ coordinate is calculated using Eq. (5.8).

By scanning the parameter space (i_{in}, i_b) while counting the number of unique fixed points, we generate Fig. 5.2. In it, there are symmetries with respect to $i_{in} = 0$ and $i_b = 0$. There is also a clear periodicity when i_{in} is varied, as expected. Note that this can become problematic as greater values of stimulus can result in quiescence in contrast to what is normally expected of a biological neuron.

The existence of fixed points does not imply a system that rests. In order to have that, there should be stable equilibria, therefore, we need to perform a stability analysis.

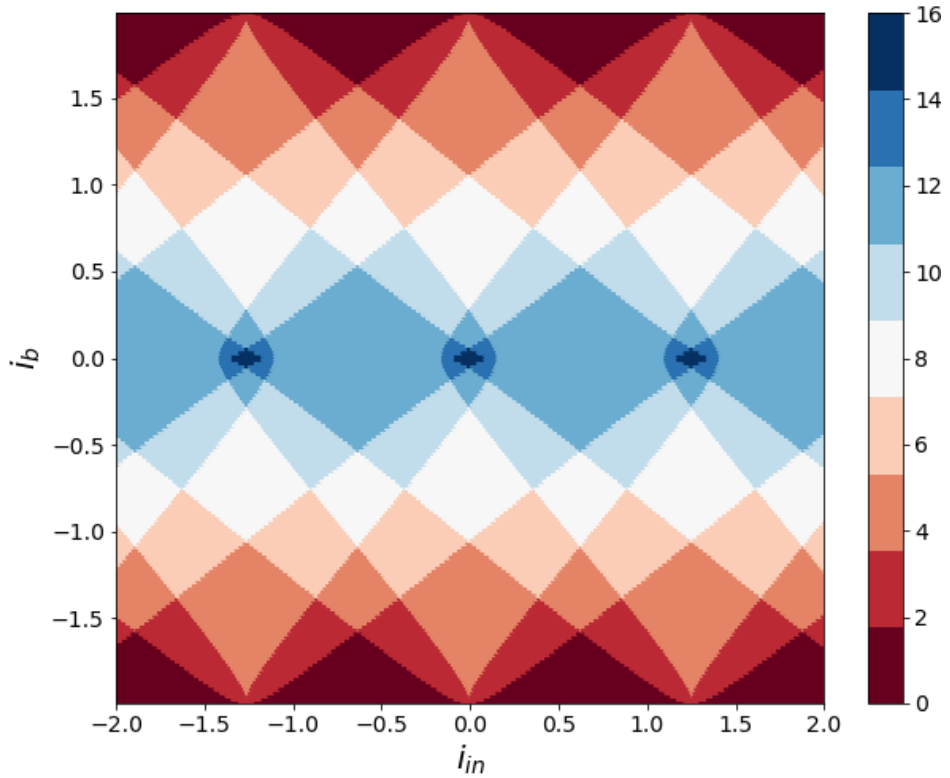

Figure 5.2: Number of fixed points provided by Eq. 5.11 for $i_{in} \in [-2, 2]$ and $i_b \in (-2, 2)$. Other parameter values as in Fig. 5.1. Independent of Γ.

Firstly, the Jacobian is calculated:

$$J = \begin{bmatrix} 0 & 1 & 0 & 0 \\ -\cos\phi_p - \lambda & -\Gamma & -\lambda & 0 \\ 0 & 0 & 0 & 1 \\ -\lambda & 0 & -\cos\phi_c - \lambda & -\Gamma \end{bmatrix}, \tag{5.12}$$

from which the determinant and the trace are found:

$$Det(J) = \cos\phi_p \cos\phi_c + \lambda(\cos\phi_c + \cos\phi_p) \tag{5.13}$$

$$Tr(J) = -2\Gamma. \tag{5.14}$$

The characteristic equation is then given by :

$$\begin{aligned} e^4 + 2e^3\Gamma + e^2[\cos\phi_p + \cos\phi_c + 2\lambda + \Gamma^2] + e\Gamma[\cos\phi_p + \cos\phi_c + 2\lambda] \\ +\lambda(\cos\phi_p + \cos\phi_c) + \cos\phi_p \cos\phi_c, \end{aligned} \tag{5.15}$$

from which, the eigenvalues are found:

$$e_1 = \frac{1}{2}(-\sqrt{-A + B} - \Gamma) \tag{5.16}$$

$$e_2 = \frac{1}{2}(\sqrt{-A + B} - \Gamma) \tag{5.17}$$

$$e_3 = \frac{1}{2}(-\sqrt{A + B} - \Gamma) \tag{5.18}$$

$$e_4 = \frac{1}{2}(\sqrt{A + B} - \Gamma), \tag{5.19}$$

where

$$A = 2\sqrt{(\cos\phi_p - \cos\phi_c)^2 + 4\lambda^2} > 0, \tag{5.20}$$

$$B = -2(\cos\phi_p + \cos\phi_c + 2\lambda) + \Gamma^2. \tag{5.21}$$

The eigenvalues confirm that $Det(J) = \prod e_i$ and $Tr(J) = \sum e_i$. An equilibrium is stable when the real parts of its eigenvalues are negative. In any other case, the fixed point is unstable. Note that Eqs. (5.16)-(5.19) do not contain i_{in}. The stimulus just moves the nullclines, it does not explicitly affect the stability of the equilibria.

Next, we want to see how the parameters i_{in} and Γ affect the transition between resting and spiking states. Thus, we need to analyze the bifurcations of the system.

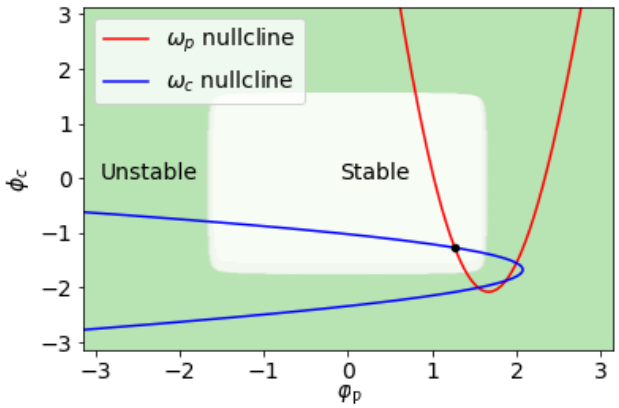

Figure 5.3: Stability of the fixed points for $i_{in} = 0$ and independent of $\Gamma > 0$. There are three unstable and one stable equilibria. The latter is denoted by a black dot. Other parameter values as in Fig. 5.1.

5.2 Bifurcations

Firstly, the bifurcations of fixed points are examined beginning with the Hopf. During this bifurcation the stability of a focus changes, meaning that a conjugate pair of its eigenvalues crosses the imaginary axes. From Eqs. (5.16) - (5.19) it is evident that either $\sqrt{-A+B}$ or $\sqrt{A+B}$ will be imaginary near the bifurcation. Therefore, Γ is the quantity that must change its sign, which is impossible as it represents a positive damping coefficient. This could restrict the simulating capabilities of the model, due to the fact that the Hopf bifurcation is linked with resonator neurons. Nonetheless, we will see that subthreshold oscillations are not impossible in a JJ neuron, although they are weak.

On the other hand, SN and SNIC bifurcations are very common. This is to be expected due to the fact that Fig. 5.2 contains only even numbers of fixed points which appear and disappear in couples. Nonetheless, a more strict proof will be provided. We remind that at both SN and SNIC bifurcation points a pair of equilibria collide (see Fig. 3.10) while exactly one eigenvalue of each fixed point must have zero real part. Figure 5.4 depicts the bifurcation diagram which is independent of Γ because it was generated from Eq. (5.11).

We need to highlight that Γ does affect the kind of equilibrium, for example if it is a node or a focus, through the eigenvalues, however, it can not change the fact that for $i_{in} = i_{in,SN} \approx 0.1850$ a stable fixed point will collide

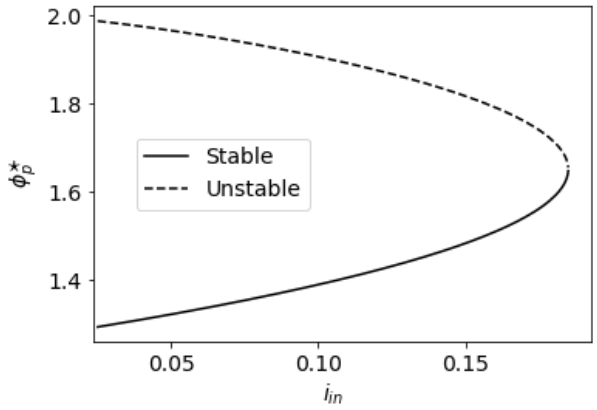

Figure 5.4: $\phi_p^\star$ dependence on i_{in} according to Eq. 5.11. Other parameter values as in Fig. 5.1. Independent of Γ.

with an unstable one. Figures 5.5 and 5.6 depict the eigenvalues of the pair of the equilibria which take part in the bifurcation for different values of Γ.

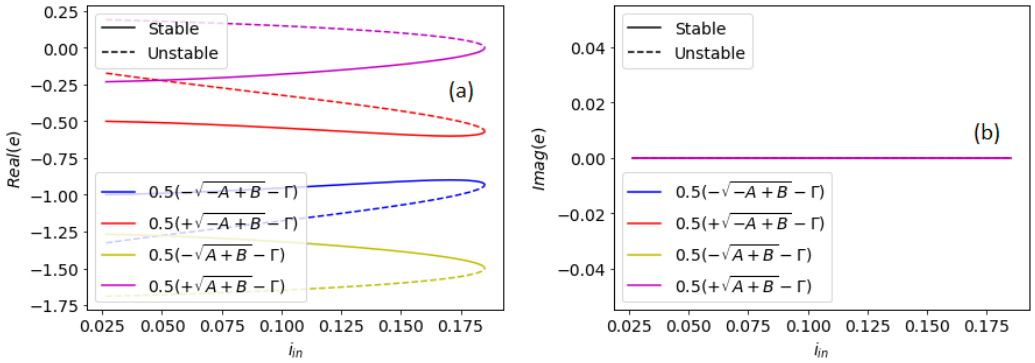

Figure 5.5: Eigenvalues near the bifurcation for $\Gamma = 1.5$. Other parameters as in Fig. 5.1. (a) Real part, (b) imaginary part.

Up to this point we have not distinguished whether the aforementioned bifurcations are SN or SNIC. In order to do that, the scaling laws of Table 3.1 are used. The analysis reveals that:

- For $\Gamma > 1.0$ the equilibria disappear through a SNIC bifurcation because right after the bifurcation point a stable LC appears, whose fre-

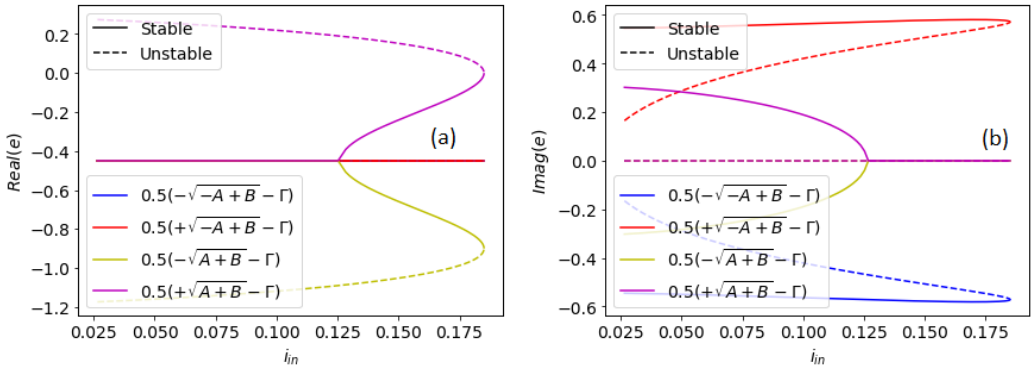

Figure 5.6: Eigenvalues near the bifurcation for $\Gamma = 0.9$. Other parameters as in Fig. 5.1. (a) Real part, (b) imaginary part.

quency follows $f \sim O(\sqrt{i_{in} - i_{in,SN}})$. Consequently, this neuron exhibits class 1 excitability. Figure 5.7 shows the scaling law for $\Gamma = 1.5$.

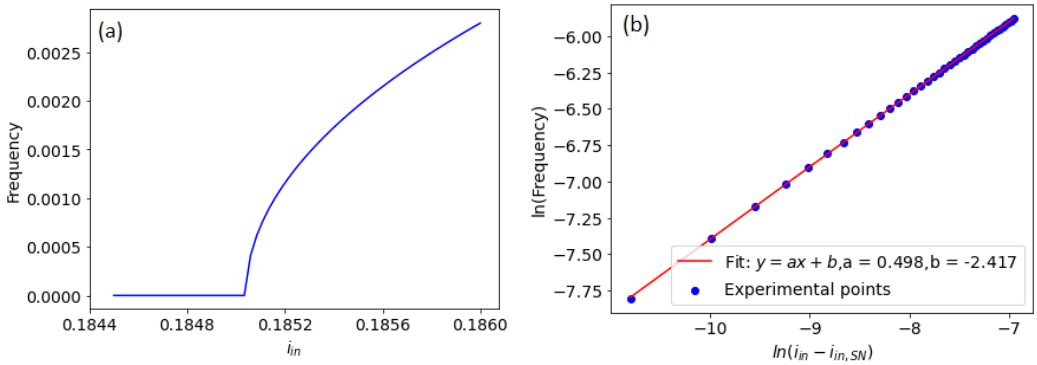

Figure 5.7: Signature of class 1 excitability. $\Gamma = 1.5$ and the other parameters as in Fig. 5.1. (a) F-I curve. (b) Linear fit right after the bifurcation. The slope approximates 0.5, verifying the scaling law.

- For $\Gamma < 1.0$ the equilibria disappear through a SN bifurcation, because right after the bifurcation point trajectories jump to an existing LC whose frequency follows $f \sim O(1)$. For $0.882 < \Gamma < 1.0$ there is also a homoclinic bifurcation at $i_{in,HOM}$ whose value is smaller than $i_{in,SN}$, through which the aforementioned stable LC is born. Near the homoclinic bifurcation the period of the LC obeys $T \sim O(\ln [i_{in} - i_{in,HOM}])$.

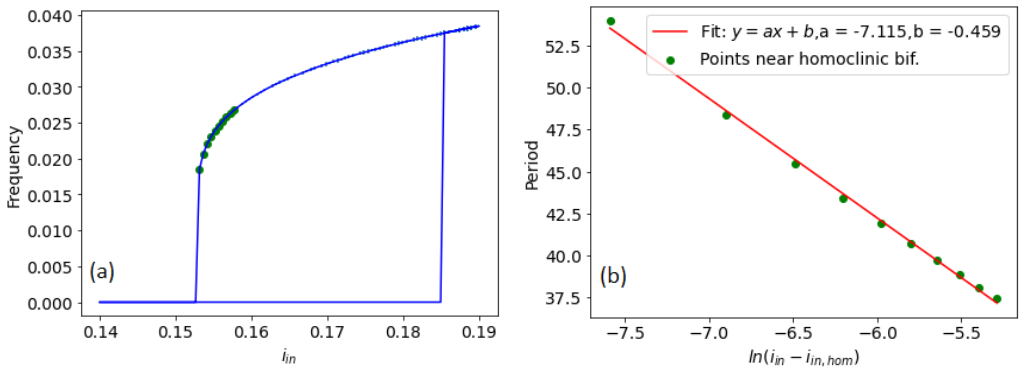

Figure 5.8: Class 2 excitability and bistability for $\Gamma = 0.9$, other parameters as in Fig. 5.1. (a) Homoclinic and SN bifurcation on the F-I curve. (b) Scaling law near the homoclinic bifurcation.

Thus, for $i_{in} \in (i_{in,HOM}, i_{in,SN})$ a LC coexists with a stable equilibrium. In this region, the neuron exhibits both class 1 spiking and class 2 excitability, which was demonstrated in Fig. 3.13. Figure 5.8 summarizes this behaviour.

It is not accidental that, for some values of Γ a homoclinic bifurcation and a SN occur nearby, nor that for greater values of Γ, a SNIC bifurcation replaces the SN one. These are the key characteristics of a SNL bifurcation which has been described in more detail in Section 3.3.4. Indeed, the stability diagram on the parameter space (i_{in}, Γ) of Fig. 5.9 is almost identical to that of Fig. 3.11.

Remember that a single JJ exhibits the same behaviour, which is shown in Fig. 4.2. The main difference is that in a single JJ, the homoclinic curve is tangent to the line $I = 4\Gamma/\pi$ as $\Gamma \to 0$ [9], while in a JJ neuron the curve tends to become parallel to the axis i_{in} for $\Gamma \to 0.881$.

The bistable regime is interesting because small perturbations of the stimulus can switch spike trains on and off resulting in a bursting-like behaviour [14]. In a circuit, this can be modelled with a stimulus: $i_{in}+\xi(t)$, where $\xi(t)$ is a white Gaussian noise with zero mean and variance σ^2. The autocorrelation function for this stochastic variable follows $\langle \xi(t)\xi(\tau) \rangle = \sigma^2 \delta(t - \tau)$.

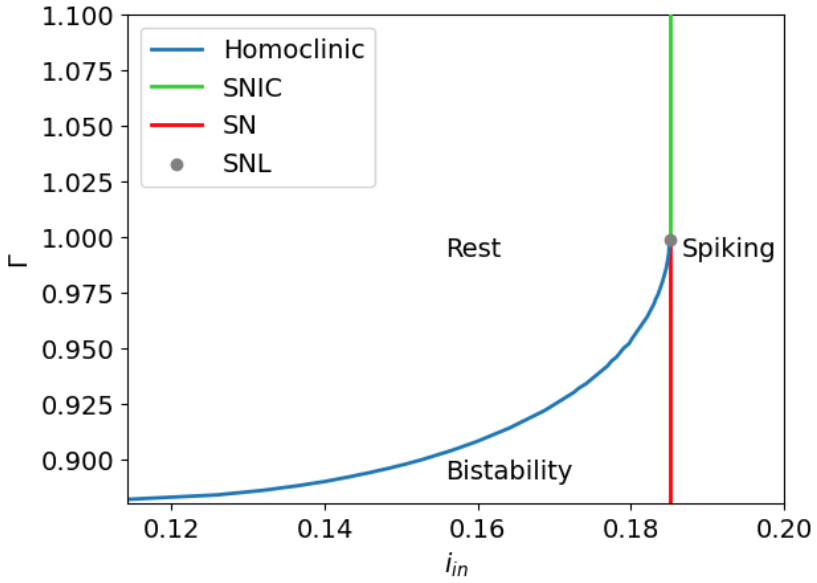

Figure 5.9: Codimension 2 bifurcation diagram for the SNL bifurcation. Other parameter values as in Fig. 5.1.

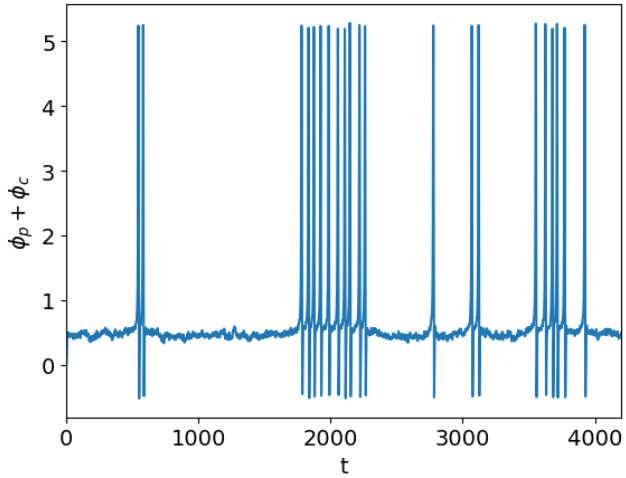

Figure 5.10: Noise-induced bursting behaviour for $\Gamma = 0.95$. Stimulus: $0.182 + \xi(t)$, where $\xi(t)$ is a Gaussian noise with standard deviation: $\sigma = 0.06$. Other parameters as in Fig. 5.1.

5.3 Additional neurocomputational properties

So far, in terms of neuronal properties, it has been verified that a JJ neuron is able to exhibit both class 1 and class 2 excitability, with the latter occurring in a bistable regime. Generally, there is a great number of neurocomputational properties corresponding to different dynamics. Some of them are shown in Table 3.2. In this section, we analyze which of them can be exhibited by the system and we explain the reason why the rest of them can not.

First of all, is should be stated again that the incapacity of the system to undergo a Hopf bifurcation does not strictly imply that a JJ neuron is an integrator, i.e, it is unable to exhibit subthreshold oscillations. This is true only for 2-dimensional systems. Indeed, Fig. 5.6 demonstrates that near the SN bifurcation, both fixed points have a pair of complex conjugate eigenvalues. For $\Gamma > 0.95$ though, the damping coefficient is too high. Consequently, when subthreshold oscillations do exist, they are negligible, as shown in Fig. 5.11a. For smaller values of Γ, more pronounced subthreshold oscillations are expected, although in this study we do not consider the case $\Gamma < 0.95$ for reasons explained in Section 5.4.

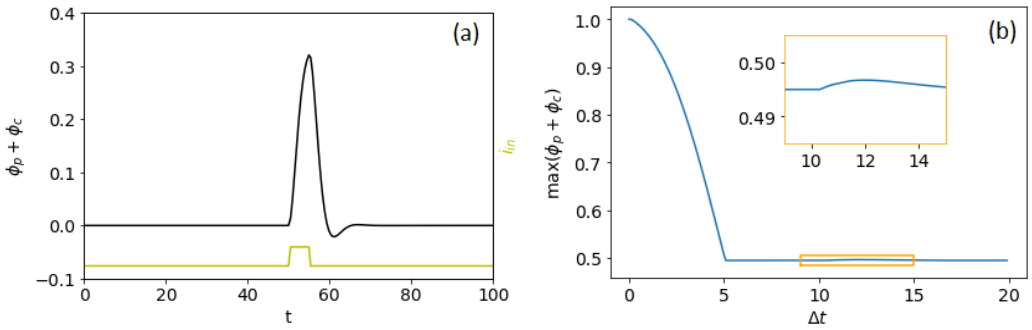

Figure 5.11: Response to different stimuli for $\Gamma = 0.95$ and other parameters as in Fig. 5.1.(a) Flux response to a subthreshold current pulse of 0.15 amplitude and width of 5. (b) Normalized maximum response to two subthreshold pulses of varied inter-pulse period Δt. The pulses are identical to that of (a). Near $\Delta t = 12$ the inset shows that the response slightly increases because the pulses resonate with the period $T = 12.03$ of the subthreshold oscillations.

As a result, the neurons we have seen so far do not display significant frequency preference. The tool which is used in order to detect this property is the normalized maximum value of $\phi_p + \phi_c$ in response to two pulses of

current with some varied delay. In the case of an integrator, the response decreases as the delay increases, while for a resonator the response increases for delays equal to multiple integers of the period. Note that effectively, the response of Fig. 5.11b is that of an integrator.

In terms of spike latency, JJ neurons of both classes 1 and 2 of excitability can exhibit it, as demonstrated in Fig. 5.12. This is expected in systems right after and very close to a SN or a SNIC bifurcation because the vector field is close to zero in the area of the annihilated fixed points. For this reason, the trajectory needs a lot of time to escape this neighborhood. Note that although both SN and SNIC bifurcations exhibit this behaviour, the frequency of the generated spikes are fundamentally different, because they belong to different classes of excitability.

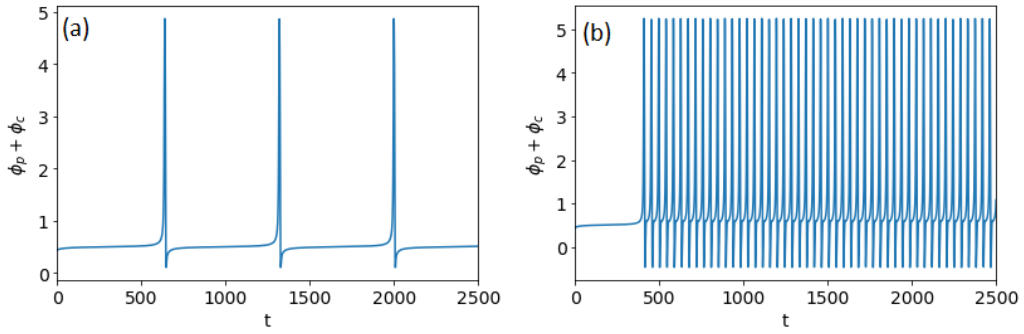

Figure 5.12: Spike latency for $i_{in} = 0.1853$ and other parameters as in Fig. 5.1. (a) $\Gamma = 1.5$ corresponding to class 1 excitability , (b)$\Gamma = 0.95$ corresponding to class 2 excitability.

Neither post-inhibitory spikes nor inhibition induced spikes are exhibited by a JJ neuron. These properties are based on the geometry of the nullclines shown in Fig. 3.14a and 3.14b which is fundamentally different than that of a JJ neuron. For $\Lambda_p = 0.5$ the quantity $\phi_p + \phi_c$ is an odd function of i_{in}, meaning that negative stimuli produces negative responses, that is spikes facing downwards.

5.4 Lyapunov exponents

Up to this point, the guide in the analysis was the behaviour of the equilibria. The only discovery concerning the behaviour of LCs was the homoclinic bifur-

cation, which was detected through the SNL bifurcation. Nonetheless, more complex dynamics are expected from a 4-dimensional system, like chaos, bifurcations of LCs and more, which can not be detected through examination of the fixed points. Thus, more sophisticated tools are needed for deeper investigation. In this thesis, the Lyapunov exponents were used.

As mentioned in section 3.3.3 the Lyapunov spectrum provides useful information about the system. In the case of a 4-dimensional dissipative system, there are 4 Lyapunov exponents: L_1, L_2, L_3, L_4, which follows:

$$\sum L_i = \vec{\nabla}\vec{f} = -2\Gamma. \tag{5.22}$$

Sorting them from the maximum to the minimum, implies that at least L_4 is negative because the sum in Eq. (5.22) is negative too. The signs of the other Lyapunov exponents we encounter, along with the corresponding dynamical behaviour are depicted in Table 5.1.

Attractor	L_1	L_2	L_3
Fixed point (FP)	$-$	$-$	$-$
Limit Cycle (LC)	0	$-$	$-$
Quasiperiodic (QP)	0	0	$-$
Chaotic (C)	$+$	0	$-$

Table 5.1: Stable attractors according to the signs of the three larger Lyapunov exponents.

The calculation of the Lyapunov spectrum is very difficult numerically. That is why a method developed by Benettin et al. was used [15]. The core idea of the algorithm, is that we follow only one trajectory along with its tangent space which is defined by the linearized equations of the system. The evolution of the system distorts a sphere defined on the tangent space into an ellipsoid whose principal axes provide the Lyapunov exponents. The repeated use of the Gram-Schmidt reorthonormalisation prevents the axes of the ellipsoid from diverging. Unfortunately, calculating the Lyapunov spectrum is time consuming. Figure 5.13 took about 10 hours to generate, hence the low resolution. Depending on the initial conditions $\vec{x_0}$, a trajectory can end up in a different attractor of the Table 5.1. We have already encountered this dependence in the bistable regime of Fig. 5.8, however, Fig. 5.13 shows that this is just the tip of the iceberg.

More specifically, Fig. 5.13b reveals an unexpectedly rich behaviour for $i_{in} < i_{in,SN}$ and $\Gamma < 1$, where chaotic or quasiperiodic attractors or LCs

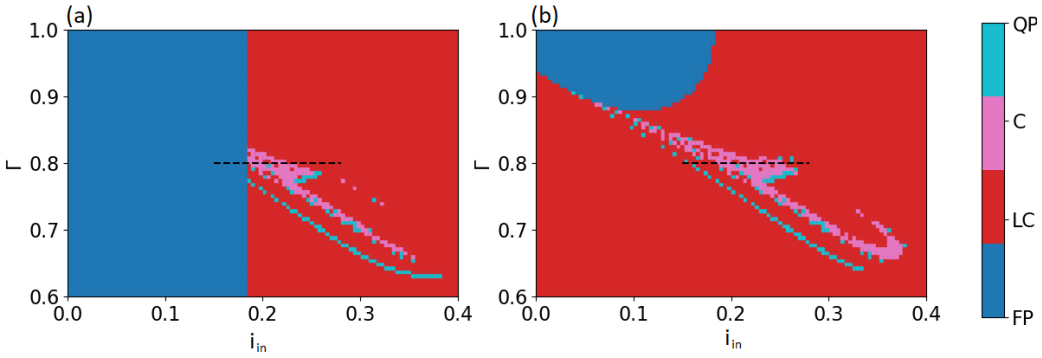

Figure 5.13: Attractors extracted from the Lyapunov spectrum. Abbreviations according to Table 5.1. The spectrum of the cross section shown by the black dashed line is depicted in Fig. 5.15. Parameters as in Fig. 5.1. (a) Using as initial conditions, either the stable fixed point: $\vec{x_0} = (\phi_p^\star, 0, \phi_c^\star, 0)$, when it exists, or the last stable fixed point before its disappearance when it does not. (b) Using $\vec{x_0} = (0, 20, 0, 0)$.

coexist with stable fixed points. The region which was expected is the transition from fixed points to LCs through the homoclinic bifurcation, whose curve starts around $(i_{in}, \Gamma) = (0.11, 0.88)$ and ends near $(0.185, 1.0)$. On the contrary, the left part of the borderline between LCs and fixed points, that is for $i_{in} < 0.11$, corresponds either to another new bifurcation, or to the movement of the basin of attraction of the LC away from the initial conditions we have chosen. Furthermore for Γ below the left part of the borderline and generally when $\Gamma < 0.88$, there is a new area of bistability which has not been investigated before. Another important discovery, is that not all LCs in this region have a spike-like form, as shown in Fig. 5.14a. Combining the aforementioned remarks, we conclude that this parameter subspace is more complicated than it seems, especially for $\Gamma < 0.95$. A more detailed analysis, which is not in the scope of this thesis, should be performed regarding the bifurcations, the basins of attraction, and the form of the trajectories..

In terms of non periodic trajectories, a sickle-like formation appears in the parameter space, formed by both chaotic and quasiperiodic regions. We should highlight, that it is difficult to distinguish these 2 behaviours due to the fact that, in the chaotic regions L_1 is close to the precision of the algorithm used for the extraction of the Lyapunov spectrum. In fact, the maximum Lypaunov exponent which was calculated for the generation of

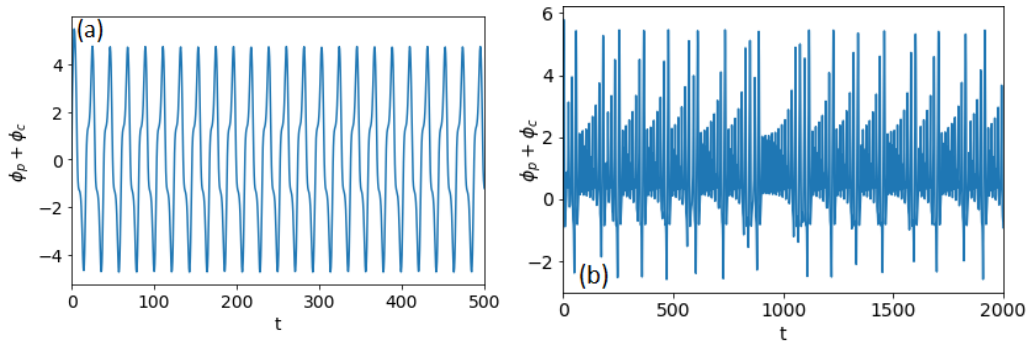

Figure 5.14: Timeseries for $\Gamma = 0.8$ and different i_{in}. Other parameters as in Fig. 5.1. (a) Non spike-like LC for $i_{in} = 0$ and initial conditions $\vec{x_0} = (0, 5, 0, 0)$. (b) Chaotic spiking for $i_{in} = 0.2$ and initial conditions $\vec{x_0} = (0, 0, 0, 0)$.

Fig. 5.13, was $max(L_1) = 0.053$, while the precision of the algorithm was set to $e = 0.005$. That means, that a Lyapunov exponent L_i is assumed zero when $|L_i| < e$. Typical chaotic spiking of a JJ neuron is depicted in Fig. 5.14b. The route from order to chaos for $\Gamma = 0.8$ is depicted in Fig. 5.15 with the help of the Lyapunov spectrum and the bifurcation diagram. In this bifurcation diagram we depict the local maxima of the $\phi_p + \phi_c$ variable over the bifurcation parameter. Observe that almost every branch of the Fig. 5.15a is continually splitting in two, until the LCs, which contain finite number of local maxima, are replaced by a chaotic attractor with infinite number of local maxima. This transition is known as the "period doubling route to chaos".

Figure 5.16 demonstrates the way the phase portrait changes as the system moves towards the chaotic regime. Due to the fact that the system is 4-dimensional it is impossible to visualise all its dimensions. We choose to depict variables $\phi_p + \phi_c$ and $\dot{\phi}_p + \dot{\phi}_c$ because they correspond to the membrane potential V and its derivative, respectively.

For $1 < \Gamma < 2$ the Lyapunov spectrum did not provide us with more information than we already have, that is, a stable fixed point that disappears through a SNIC bifurcation as i_{in} increases.

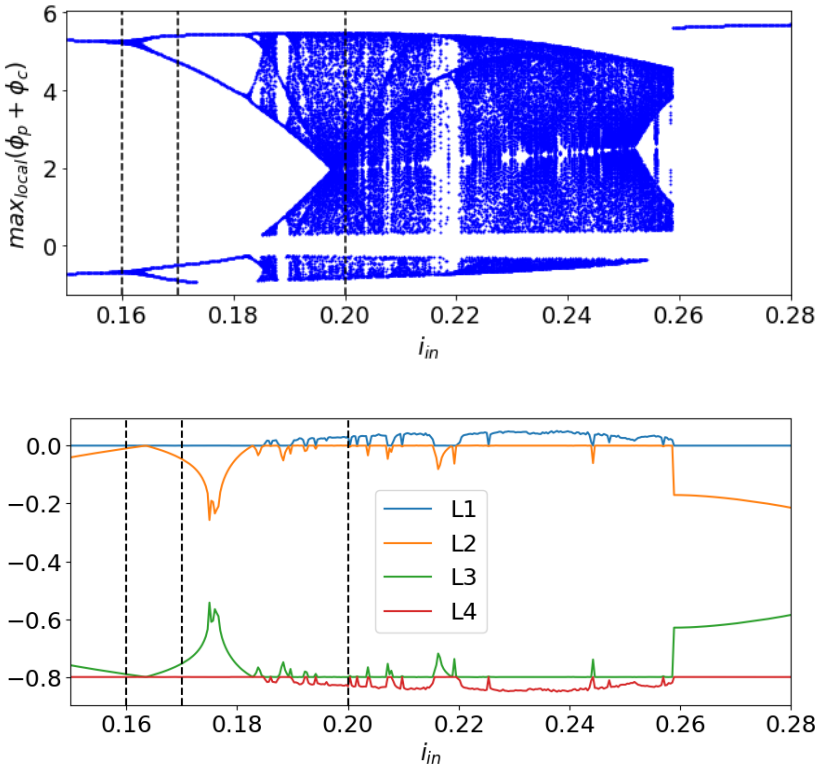

Figure 5.15: Transition between chaos and LCs for $\Gamma = 0.8$, marked by the horizontal dashed line of Fig. 5.13. Other parameters as in Fig. 5.1 and $\vec{x_0} = (0, 20, 0, 0)$. The phase portraits at the vertical dashed lines are depicted in Fig. 5.16. (a) Bifurcation diagram. (b) Lyapunov spectrum.

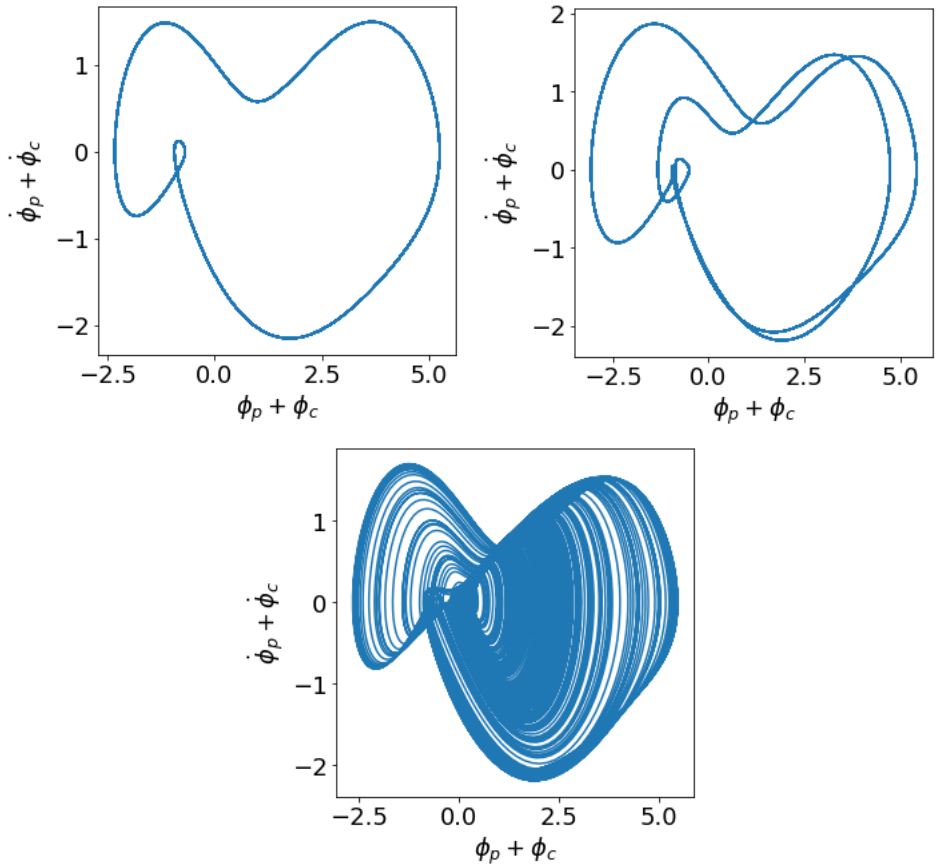

Figure 5.16: Phase portraits for $\Gamma = 0.8$ and (a) $i_{in} = 0.16$, (b) $i_{in} = 0.17$, (c) $i_{in} = 0.2$, marked by the vertical dashed lines in Fig. 5.15. Other parameters as in Fig. 5.1 and initial conditions: $\vec{x_0} = (0, 20, 0, 0)$.

Chapter 6

Conclusions and outlook

Josephson Junction (JJ) neurons are promising candidates as building blocks for large scale neuromorphic computers due to their capacity to operate in great speeds and with low energy dissipation. For this reason, their dynamical behaviour must be fully understood and compared with that of biological neurons. Previous works have already mentioned that the ability of the JJ neuron to exhibit classes of excitability 1 and 2 is due to the fact that the system undergoes saddle-node (SN) and saddle node on invariant circle (SNIC) bifurcations respectively, depending on its parameters [6].

By performing a detailed bifurcation analysis, we confirm the aforementioned behaviour, which is summarized in a codimension-2 bifurcation called Saddle Node Loop (SNL). The SNL bifurcation occurs near $(i_{in}, \Gamma) = (0.185, 1.0)$ with the other parameters kept fixed, as in the literature $(\lambda, \Lambda_p, \Lambda_c, i_b) = (0.1, 0.5, 0.5, 1.909)$. SNL bifurcations are found in neuronal models and are linked with a variety of neurocomputational properties. More specifically, all properties shown in Fig. 6.1, apart from chaotic spiking, were expected. In addition to the SNL bifurcation, the system exhibits more complex behaviour for $\Gamma < 1.0$, in particular, chaotic spiking, which occurs through a series of period doubling bifurcations as i_{in} increases, the so-called period doubling route to chaos.

Besides the neuromorphic properties of the JJ neuron, we have found two behaviours beyond biological relevance which should be further studied:

- Firstly, Fig. 5.2 shows that the number of the fixed points is a periodic function of i_{in}. Thus, it is possible that a neuron will stop spiking because its stimulus increases, an unusual neuronal behaviour to our

knowledge. Possible future work could study the maximum input a neuron can receive in experimental conditions.

- Secondly, great care should be taken for $\Gamma < 1.0$. Figure 5.13 reveals the existence of non expected limit cycles which do not have the correct spike-like form, as in Fig. 5.14a. Future work could investigate them more and check if different values of the parameters (i_b, Λ_p) could eliminate them. In this way, we will be able to safely use JJ neurons which exhibit class 2 excitability or chaotic spiking. Furthermore, for smaller values of Γ we expect neurons to exhibit frequency preference, a very important neurocomputational property.

Finally, future investigation could concern the emulation of bursting, a behaviour which was only briefly touched in this thesis. Bursting neurons fire a burst of spikes periodically followed by a period of quiescence [9]. Dynamically, bursting requires at least one additional dimension, because a new variable should switch on and off the spiking generated from the other variables of the system. Biologically, that occurs through slower currents while a JJ neuron could burst either by adding more electrical components to the circuit, or by coupling i_b current with some variable of the system.

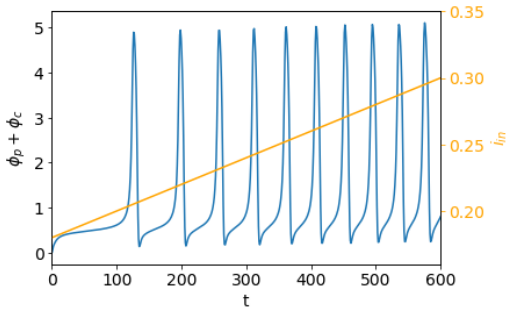

Class 1 Spiking. (params. as Fig. 5.7.)

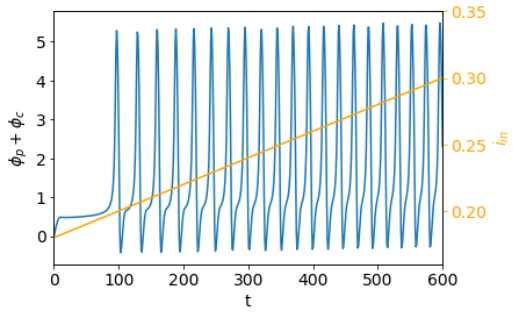

Class 2 Spiking. (params. as Fig. 5.8.)

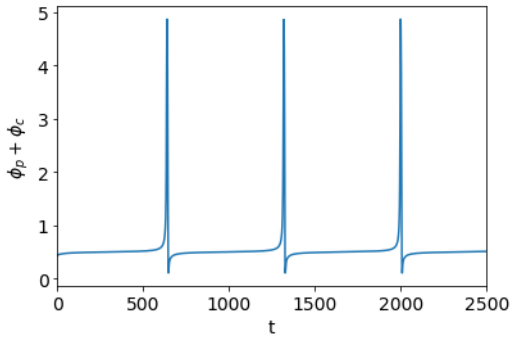

Spike Latency for class 1 (Fig. 5.12b).

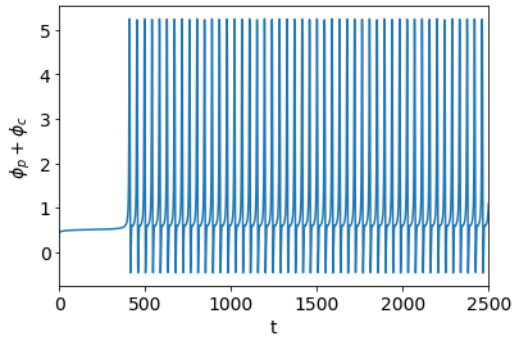

Spike Latency for class 2 (Fig. 5.12a).

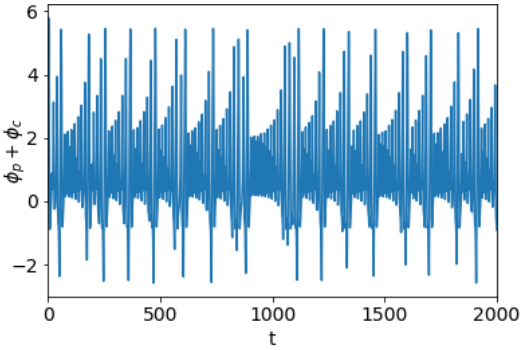

Chaotic Spiking (Fig. 5.14b).

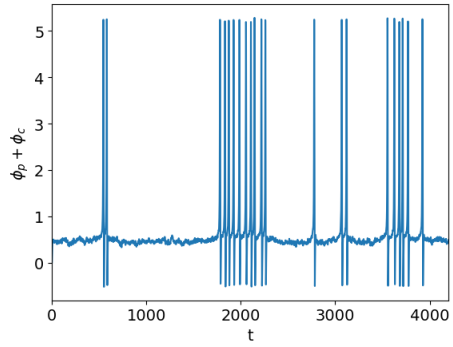

Noise induced bursting (Fig. 5.10).

Figure 6.1: Summary table of the neurocomputational properties exhibited by a JJ neuron.

Appendix A

Generation of a spike in a Josepshon Junction neuron

In this part, we explain in detail the generation of the spikes in a JJ neuron. We rewrite Eqs. (5.1)-(5.2) but we now interpret them as 2 coupled, driven and damped pendula:

$$\ddot{\phi}_p + \Gamma\dot{\phi}_p + \sin\phi_p = -\lambda(\phi_c + \phi_p) + \Lambda_s i_{in} + (1 - \Lambda_p)i_b = i_p \tag{A.1}$$

$$\ddot{\phi}_c + \Gamma\dot{\phi}_c + \sin\phi_c = -\lambda(\phi_c + \phi_p) + \Lambda_s i_{in} - \Lambda_p i_b = i_c, \tag{A.2}$$

where Γ is the damping coefficient, i_p is the torque driving the "p" pendulum, i_c is the torque driving the "c" pendulum, λ is the coupling coefficient and i_{in} simulates the external stimulus. The parameter values which are used in this demonstration are: $\Gamma = 1.5$, $L_p = 0.5$, $L_s = 0.5$, $\lambda = 0.1$, $i_b = 1.909$ and

$$i_{in} = \begin{cases} 0, & \text{if } t \leq 30 \\ 0.21, & \text{if } t > 30. \end{cases}$$

The different stages during the generation of a spike are visualised in Fig. A.1. For $i_{in} = 0$ the bias torque i_b forces both pendula to rest in some non zero angles with opposite sign ($t = 21.0$). When i_{in} comes into play, both i_p and i_c increase. Initially, this results in a slow increase of ϕ_p, while ϕ_c is almost unaffected (see $t = 45.0$). At some point, the role of gravity in the movement of pendulum "p" switch sides, from constraining to enhancing it ($t = 85.0$). For this reason the pendulum whirls quickly ($t = [85.0, 95.0]$). The abrupt

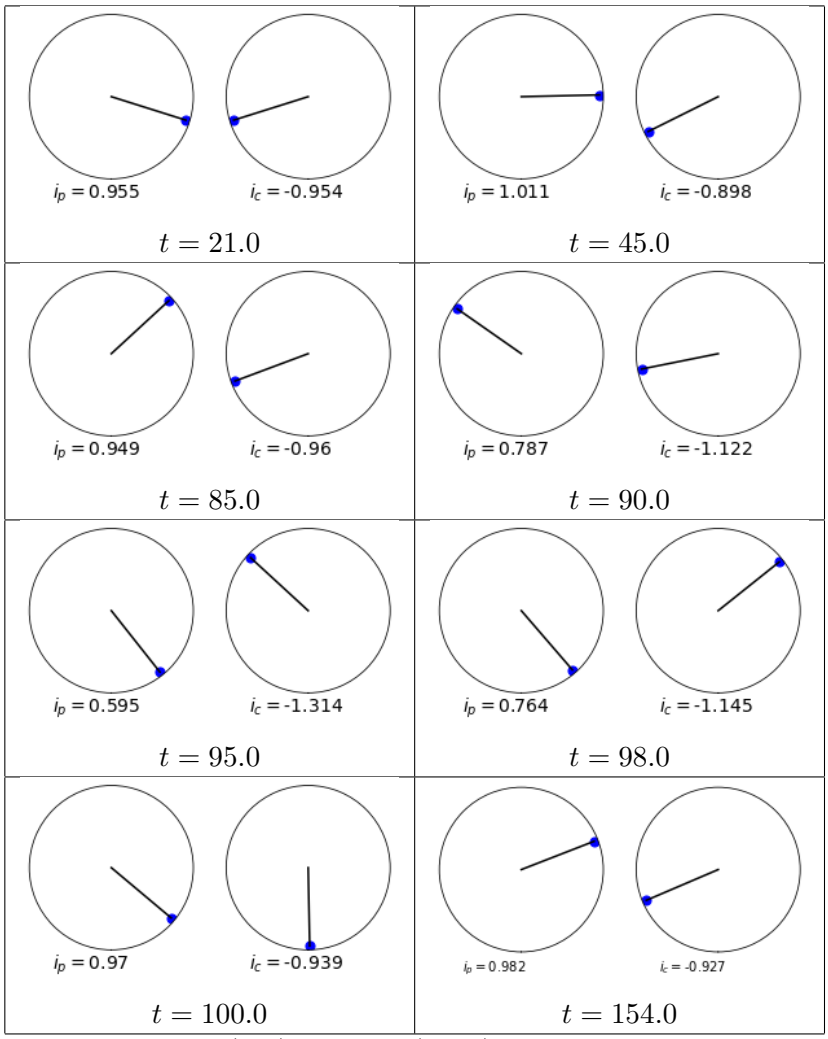

Figure A.1: Pendula "p" (left) and "c" (right) for different timesteps along with the torque i_p and i_c they experience, respectively.

increase of ϕ_p makes the term $-\lambda(\phi_p + \phi_c)$ important. Consequently, both i_p and i_c decrease rapidly. This change alongside with gravity, which has switched sides again, slows down ϕ_p to an almost resting situation. At the same time, pendulum "c" whirls over in the opposite direction then that of "p" ($t = [95.0, 100.0]$). When both pendula have whirled once, the $-\lambda(\phi_p+\phi_c)$ term becomes negligible again. It takes a lot of time for pendulum "p" to arrive at the whirling point ($t = [100.0, 154.0]$) for a second time, where the whole procedure will repeat. In Fig. A.2 we keep track of ϕ_p,ϕ_c and ϕ_p+ϕ_c.

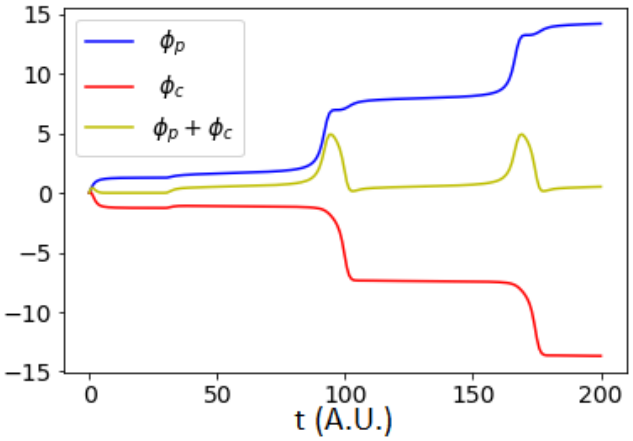

Figure A.2: Time evolution of the spike along with its components ϕ_p and ϕ_c. Other parameters: $\Gamma = 1.5$, $L_p = 0.5$, $L_s = 0.5$, $\lambda = 0.1$, $i_b = 1.909$.

Appendix B

Numerical tools

For the needs of this thesis, code was developed in Python and Julia programming languages. More specifically:

- Julia was used for time intensive tasks because it is much faster than Python. Furthermore, its libraries "DifferentialEquations.jl" and "DynamicalSystems.jl" contain useful functions, especially those that perform numerical integration and generate the Lyapunov spectrum [16, 17]. For these two functions the methods which were used were: "Tsitouras 5/4 Runge-Kutta" for the former [18], and a method developed be Benettin and others for the latter [15]. Figures 5.9, 5.10, 5.13 and 5.15b were generated in Julia.

- The biggest portion of the code was developed in Python. The rest of the figures which were not mentioned above were generated with this programming language. For the numerical integration the "integrate.solve_ivp" function from "scipy" library was used [19], which also employs a Runge-Kutta method [20].

A great variety of original functions were generated in both programming languages. Some of them are: a frequency calculator, a function which matches the Lyapunov spectrum to its attractor and functions calculating the analytical quantities of the system, such as the fixed points. For more details, the code is available at the github page: https://github.com/gerompampastrumf/JJ_neuron.git.

Bibliography

[1] Danijela Marković et al. "Physics for neuromorphic computing". In: *Nature Reviews* (2020).

[2] Steve Furber. "Large-scale neuromorphic computing systems". In: *Journal of Neural Engineering* (2016).

[3] Mishra Arindam et al. "Neuron-like spiking and bursting in Josephson junctions: A review". In: *Chaos: An Interdisciplinary Journal of Nonlinear Science* (2021).

[4] Emily Toomey, Ken Segall, and Karl K. Berggren. "Design of a Power Efficient Artificial Neuron Using Superconducting Nanowires". In: *Frontiers in Neuroscience* (2019).

[5] Matteo Castellani. "Design of Superconducting Nanowire-Based Neurons and Synapses for Power-Efficient Spiking Neural Networks". Politecnico di Torino, 2020.

[6] Patrick Crotty, Dan Schult, and Ken Segall. "Josephson junction simulation of neurons". In: *Physical Review E* (2010).

[7] Kenneth Segall et al. "Synchronization dynamics on the picosecond time scale in coupled Josephson junction neurons". In: *Physica B: Condensed Matter* (2014).

[8] Wulfram Gerstner, Richard Naud Werner M. Kistler, and Liam Paninski. *Neuronal Dynamics: From Single Neurons to Networks and Models of Cognition*. Cambridge Universtiy Press, 2014. ISBN: 9781107635197.

[9] Eugene M. Izhikevich. *Dynamical Systems in Neuroscience: The Geometry of Excitability and Bursting*. MIT Press, 2006. ISBN: 9780262090438.

[10] Dee U. Silverthorn. *Human Physiology: An Integrated Approach (7th Edition)*. Pearson, 2016. ISBN: 9780130176974.

[11] Steven H. Strogatz. *Nonlinear dynamics and chaos: with applications to physics, biology, chemistry and engineering*. Perseus Books Publishing, 1994. ISBN: 9780813349107.

[12] Alan Wolf et al. "Determining Lyapunov exponents from a time series". In: *Physica D* (1984).

[13] Yuri A. Kuznetsov. *Elements of Applied Bifurcation Theory*. Springer, 2004. ISBN: 9780387983820.

[14] Jan-Hendrik Schleimer et al. "Firing statistics in the bistable regime of neurons with homoclinic spike generation". In: *Physical Review E* (2021).

[15] Giancarlo Benettin et al. "Lyapunov Characteristic Exponents for Smooth Dynamical Systems and for Hamiltonian Systems; A Method for Computing All of Them. Part 1: Theory". In: *Meccanica* (1980).

[16] Christopher Rackauckas and Qing Nie. "Differentialequations.jl–a performant and feature-rich ecosystem for solving differential equations in julia". In: *Journal of Open Research Software* 5.1 (2017).

[17] George Datseris. "DynamicalSystems.jl: A Julia software library for chaos and nonlinear dynamics". In: *Journal of Open Source Software* 3.23 (2018), p. 598.

[18] Charalampos Tsitouras. "Runge-Kutta Pairs of Orders 5(4) using the Minimal Set of Simplifying Assumptions". In: *AIP Conference Proceedings* 1168 (Sept. 2009).

[19] Pauli Virtanen et al. "SciPy 1.0: Fundamental Algorithms for Scientific Computing in Python". In: *Nature Methods* 17 (2020), pp. 261–272.

[20] J.R. Dormand and P.J. Prince. "A family of embedded Runge-Kutta formulae". In: *Journal of Computational and Applied Mathematics* 6.1 (1980), pp. 19–26. ISSN: 0377-0427.